Astronomy & Astrophysics manuscript no. a1240new8
May 19, 2009

Internal dynamics of Abell 1240: a galaxy cluster with symmetric double radio relics

R. Barrena[1], M. Girardi[2,3], W. Boschin[4,2], and M. Dasí[5,1]

[1] Instituto de Astrofísica de Canarias, C/Vía Láctea s/n, E-38205 La Laguna (Tenerife), Canary Islands, Spain

[2] Dipartimento di Astronomia of the Università degli Studi di Trieste, via Tiepolo 11, I-34143 Trieste, Italy

[3] INAF - Osservatorio Astronomico di Trieste, via Tiepolo 11, I-34143 Trieste, Italy

[4] Fundación Galileo Galilei - INAF, Rambla José Ana Fernández Perez 7, E-38712 Breña Baja (La Palma), Canary Islands, Spain

[5] Max-Planck-Institut für Sonnensystemforschung, Max-Planck-Str. 2, G-37191 Katlenburg-Lindau, Germany

Received / Accepted

ABSTRACT

Context. The mechanisms giving rise to diffuse radio emission in galaxy clusters, and in particular their connection with cluster mergers, are still debated.
Aims. We aim to obtain new insights into the internal dynamics of the cluster Abell 1240, showing the presence of two roughly symmetric radio relics, separated by $\sim 2\ h_{70}^{-1}$ Mpc.
Methods. Our analysis is mainly based on redshift data for 145 galaxies mostly acquired at the Telescopio Nazionale Galileo and on new photometric data acquired at the Isaac Newton Telescope. We also use X–ray data from the Chandra archive and photometric data from the Sloan Digital Sky Survey (Data Release 7). We combine galaxy velocities and positions to select 89 cluster galaxies and analyze the internal dynamics of the Abell 1237 + Abell 1240 cluster complex, being Abell 1237 a close companion of Abell 1240 towards the southern direction.
Results. We estimate similar redshifts for Abell 1237 and Abell 1240, $\langle z \rangle = 0.1935$ and $\langle z \rangle = 0.1948$, respectively. For Abell 1237 we estimate a line–of–sight (LOS) velocity dispersion $\sigma_V \sim 740$ km s^{-1} and a mass $M \sim 6 \times 10^{14}\ h_{70}^{-1}\ M_\odot$. For Abell 1240 we estimate a LOS $\sigma_V \sim 870$ km s^{-1} and a mass range $M \sim 0.9 - 1.9 \times 10^{15}\ h_{70}^{-1}\ M_\odot$, which takes into account its complex dynamics. Abell 1240 is shown to have a bimodal structure with two galaxy clumps roughly defining the N–S direction, the same one defined by the elongation of its X–ray surface brightness and by the axis of symmetry of the relics. The two brightest galaxies of Abell 1240, associated to the northern and southern clumps, are separated by a LOS rest–frame velocity difference $V_{rf} \sim 400$ km s^{-1} and by a projected distance $D \sim 1.2\ h_{70}^{-1}$ Mpc. The two–body model agrees with the hypothesis that we are looking at a cluster merger occurred largely in the plane of the sky, with the two galaxy clumps separated by a rest–frame velocity difference $V_{rf} \sim 2000$ km s^{-1} at a time of 0.3 Gyrs after the crossing core, while Abell 1237 is still infalling onto Abell 1240. Chandra archive data confirm the complex structure of Abell 1240 and allow us to estimate a global X–ray temperature $T_X = 6.0 \pm 0.5$ keV.
Conclusions. In agreement with the findings from radio data, our results for Abell 1240 strongly support the "outgoing merger shocks" model to explain the presence of the relics.

Key words. Galaxies: clusters: individual: Abell 1240, Abell 1237 – Galaxies: clusters: general – Galaxies: kinematics and dynamics

1. Introduction

Merging processes constitute an essential ingredient of the evolution of galaxy clusters (see Feretti et al. 2002b for a review). An interesting aspect of these phenomena is the possible connection of cluster mergers with the presence of extended, diffuse radio sources: halos and relics. The synchrotron radio emission of these sources demonstrates the existence of large–scale cluster magnetic fields and of widespread relativistic particles. Cluster mergers have been suggested to provide the large amount of energy necessary for electron reacceleration up to relativistic energies and for magnetic field amplification (Feretti 1999; Feretti 2002a; Sarazin 2002). Radio relics ("radio gischts" as referred by Kempner et al. 2003), which are polarized and elongated radio sources located in the cluster peripheral regions, seem to be directly associated with merger shocks (e.g., Ensslin et al. 1998; Roettiger et al. 1999; Ensslin & Gopal–Krishna 2001; Hoeft et al. 2004). Radio halos, unpolarized sources which permeate the cluster volume similarly to the X–ray emitting gas, are more likely to be associated with the turbulence following a cluster merger (Cassano & Brunetti 2005). However, the precise radio halos/relics formation scenario is still debated since the diffuse radio sources are quite uncommon and only recently one can study these phenomena on the basis of a sufficient statistics (few dozen clusters up to $z \sim 0.3$, e.g., Giovannini et al. 1999; see also Giovannini & Feretti 2002; Feretti 2005a) and attempt a classification (e.g., Kempner et al. 2003; Ferrari et al. 2008).

There is growing evidence of the connection between diffuse radio emission and cluster merging, since up to now diffuse radio sources have been detected only in merging systems. In

Send offprint requests to: R. Barrena, e-mail: rbarrena@iac.es

most of the cases the cluster dynamical state has been derived from X–ray observations (see Buote 2002; Feretti 2006 and 2008 and refs. therein). Optical data are a powerful way to investigate the presence and the dynamics of cluster mergers (e.g., Girardi & Biviano 2002), too. The spatial and kinematical analysis of member galaxies allow us to detect and measure the amount of substructure, to identify and analyze possible pre–merging clumps or merger remnants. This optical information is really complementary to X–ray information since galaxies and intra–cluster medium react on different time scales during a merger (see, e.g., numerical simulations by Roettiger et al. 1997). In this context we are conducting an intensive observational and data analysis program to study the internal dynamics of clusters with diffuse radio emission by using member galaxies (Girardi et al. 2007 and refs. therein [1]).

During our observational program we have conducted an intensive study of the cluster Abell 1240 (hereafter A1240).

A1240 is a very rich, X–ray luminous, Abell cluster: Abell richness class = 2 (Abell et al. 1989); L_X(0.1–2.0 keV)=$8.3\times10^{43}\ h_{70}^{-2}$ erg s^{-1} recovered from ROSAT data (David et al. 1999, correcting for our cluster redshift, see below). Optically, the cluster center is not dominated by any single galaxy – it is classified as Bautz–Morgan class III (Abell et al. 1989).

Kempner & Sarazin (2001) revealed the presence of two roughly symmetric radio relics from the Westerbork Northern Sky Survey. They appear to either side of the cluster center, north and south, at distances of $\sim 6'$ and $7'$. Kempner & Sarazin also noticed that A1240 shows an elongated X–ray morphology (recovered from ROSAT observations) consistent with a slightly asymmetric merger with the apparent axis roughly aligned with the axis of symmetry of the relics (see also Bonafede et al. 2009). The presence of double relics was confirmed by recent, deep VLA observations (Bonafede et al. 2009; see Fig. 1). Very few other clusters with double relics have been observed: Abell 3667 (Röttgering et al. 1997), Abell 3376 (Bagchi et al. 2006), Abell 2345 (Giovannini et al. 1999; Bonafede et al. 2009) and RXCJ 1314.4–2515 (Feretti et al. 2005b; Venturi et al. 2007). The relics of Abell 3667 were explained with the "outgoing merger shocks" model (Roettiger et al. 1999). Observations of Abell 3376 agree with both the "outgoing merger shocks" and the "accretion shocks" models (Bagchi et al. 2006). In the case of Abell 2345 the observations are difficult to reconcile with theoretical scenarios (Bonafede et al. 2009). Instead, more data are needed for RXCJ 1314.4–2515 (Feretti et al. 2005b and Venturi et al. 2007). As for A1240, the detailed analysis of its radio properties is in agreement with the "outgoing merger shocks" (Bonafede et al. 2009), but the main global properties are unknown and the internal cluster dynamics was never studied.

Indeed, few spectroscopic data have been reported in the field of A1240 (see NED) and the value usually quoted in the literature for the cluster redshift ($z = 0.159$; see, e.g., David et al. 1999) is given by Ebeling et al. (1996), on the basis of the 10th–ranked cluster galaxy. The real cluster redshift, as estimated in this paper, is rather $z = 0.195$. Even poorer information is known for Abell 1237 (hereafter A1237), a close southern companion of A1240, having richness class = 1 and Bautz–Morgan class III (Abell et al. 1989).

Recently, we performed spectroscopic and photometric observations of the A1237+A1240 complex with the Telescopio Nazionale Galileo (TNG) and the Isaac Newton Telescope (INT), respectively. Our present analysis is mainly based on our new optical data and X–ray Chandra archival data. We also use the few public redshifts and photometric data from the Sloan Digital Sky Survey (SDSS, Data Release 7). This paper is organized as follows. We present our new optical data and the cluster catalog in Sect. 2. We present our results about the cluster structure based on optical and X–ray data in Sects. 3 and 4, respectively. Finally, we briefly discuss our results and give our conclusions in Sects. 5 and 6.

Unless otherwise stated, we give errors at the 68% confidence level (hereafter c.l.). Results with a c.l. below 90% are considered very poorly/no significant. The values of these c.ls. are generally not explicitly listed throughout the paper.

Throughout this paper, we use $H_0 = 70$ km s^{-1} Mpc^{-1} in a flat cosmology with $\Omega_0 = 0.3$ and $\Omega_\Lambda = 0.7$. In the adopted cosmology, $1'$ corresponds to $\sim 194\ h_{70}^{-1}$ kpc at the cluster redshift.

2. New data and galaxy catalog

Multi–object spectroscopic observations of A1240 were carried out at the TNG telescope in December 2006 and December 2007. We used DOLORES/MOS with the LR–B Grism 1, yielding a dispersion of 187 Å/mm. In December 2006 we used the old Loral CCD, with a pixel size of 15 μm, while in December 2007 we used the new E2V CCD, with a pixel size of 13.5 μm. Both the CCDs are matrices of 2048×2048 pixels. In total we observed four MOS masks (2 in 2006 and 2 in 2007) for a total of 142 slits. We acquired three exposures of 1800 s for each mask. Wavelength calibration was performed using Helium–Argon lamps. Reduction of spectroscopic data was carried out with the IRAF [2] package.

Radial velocities were determined using the cross–correlation technique (Tonry & Davis 1979) implemented in the RVSAO package (developed at the Smithsonian Astrophysical Observatory Telescope Data Center). Each spectrum was correlated against six templates for a variety of galaxy spectral types: E, S0, Sa, Sb, Sc, Ir (Kennicutt 1992). The template producing the highest value of $\mathcal{R}$, i.e., the parameter given by RVSAO and related to the signal–to–noise ratio of the correlation peak, was chosen. Moreover, all spectra and their best correlation functions were examined visually to verify the redshift determination. In 4 cases (IDs 55, 61, 69, 129, 137; see Table 1) we took the EMSAO redshift as a reliable estimate of the redshift. Our spectroscopic survey in the field of A1240 consists of spectra for 118 galaxies with a median nominal error on cz of 50 km s^{-1}. The nominal errors as given by the cross–correlation are known to be smaller than the true errors (e.g., Malumuth et al. 1992; Bardelli et al. 1994; Ellingson & Yee 1994; Quintana et al. 2000; Boschin et al. 2004). Double redshift determinations for four galaxies allowed us to estimate real intrinsic errors. We compared the first and second determinations computing the mean and the rms of the variable $(z_1 - z_2)/\sqrt{err_1^2 + err_2^2}$. We obtained $mean = 0.3 \pm 1.4$ and $rms = 2.8$, to be compared with the expected values of 0 and 1. The resulting mean shows that the two sets of measurements are consistent with having the same velocity zero–point. According to the χ^2–test the high value of the rms suggests that the errors are underestimated. Only when nominal errors are multiplied by a ~ 2 factor the rms is in acceptable agreement with the value

[1] please visit the web site of the DARC (Dynamical Analysis of Radio Clusters) project: http://adlibitum.oat.ts.astro.it/girardi/darc.

[2] IRAF is distributed by the National Optical Astronomy Observatories, which are operated by the Association of Universities for Research in Astronomy, Inc., under cooperative agreement with the National Science Foundation.

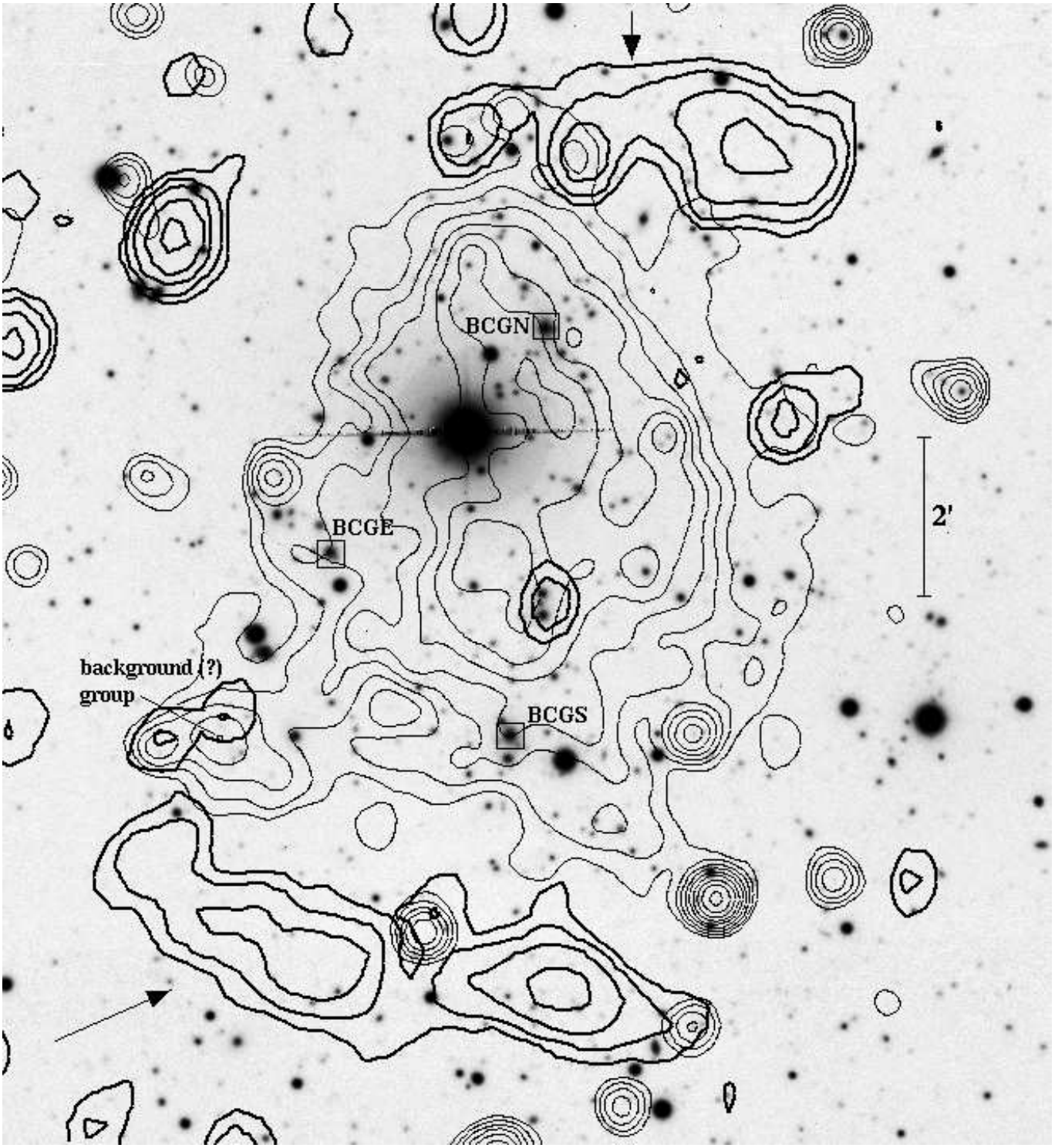

Fig. 1. INT *R*–band image of the cluster A1240 (North at the top and East to the left) with, superimposed, the contour levels of the Chandra archival image ID 4961 (thin contours; photons in the energy range 0.5–2 keV) and the contour levels of a VLA radio image at 1.4 GHz (thick contours; Bonafede et al 2009). Arrows show the positions of the two radio relics. Boxes highlight the brightest galaxies of A1240: BCGN, BCGS and BCGE (see text).

of 1. Therefore, hereafter we assume that true errors are larger than nominal cross–correlation errors by a factor 2. For the four galaxies with two redshift estimates we used the weighted mean of the two measurements and the corresponding errors.

We also use 32 public redshift data as taken from NED within a box of 45x45′ from the cluster center. They come from the SDSS (Data Release 7). Before to proceed with the merging between our and published catalogs we payed particular attention to their compatibility. Five galaxies are in common between SDSS and TNG data. For them we computed the mean and the rms of the variable $(z_{\rm our} - z_{\rm lit})/\sqrt{err^2_{\rm our} + err^2_{\rm lit}}$. We obtained $mean = -0.1 \pm 0.6$ and $rms = 1.5$, to be compared with the expected values of 0 and 1. The resulting mean shows that the two

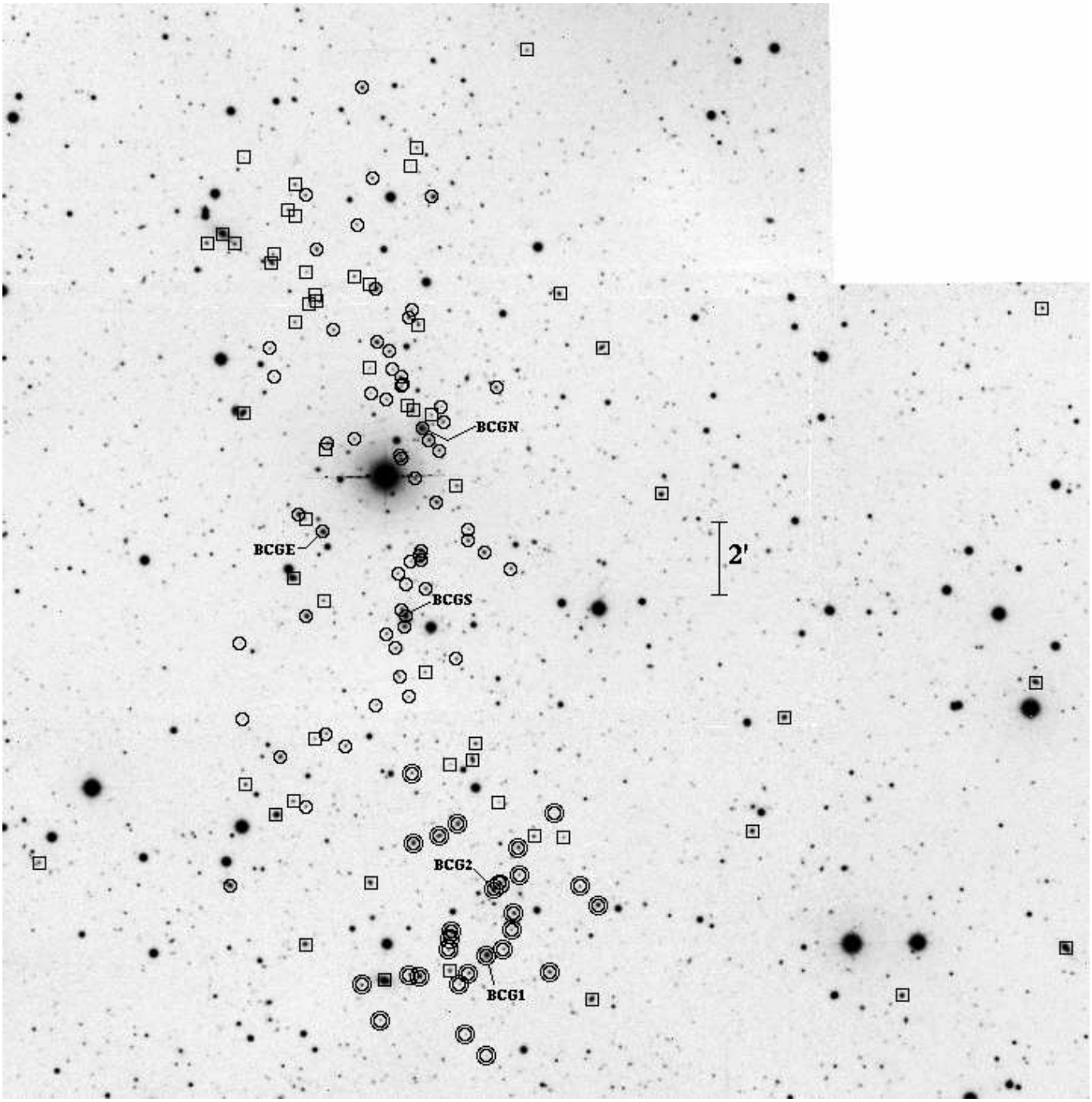

Fig. 2. INT *R*–band image of the A1237+A1240 complex (North at the top and East to the left). Circles and annuli indicate cluster members of A1240 and A1237, respectively (see Table 1). Boxes indicate non–member galaxies.

sets of measurements are consistent with having the same velocity zero–point, and the value of rms is compatible with a value of 1 according to the χ^2–test. Thus we added the redshifts coming from the literature. For the five galaxies in common we used the weighted mean of the two redshift determinations and the corresponding errors. We obtained a final catalog of 145 galaxies with measured radial velocities.

As far as photometry is concerned, our observations were carried out with the Wide Field Camera (WFC), mounted at the prime focus of the 2.5m INT telescope. We observed the A1237+A1240 complex with $B_{\rm H}$ and $R_{\rm H}$ in photometric conditions. The *R* image was obtained in December 19th 2004 with a seeing condition of 3.0″. We got the *B* image in May 14th 2006 with a seeing of about 1.1″.

The WFC consists of a four–CCD mosaic covering a 33′×33′ field of view, with only a 20% marginally vignetted area. We took nine exposures of 720 s in $B_{\rm H}$ and 300 s in $R_{\rm H}$ Harris filters (a total of 6480 s and 2700 s in each band) developing a dithering pattern of nine positions. This observing mode allowed us to build a "supersky" frame that was used to correct our images for fringing patterns (Gullixson 1992). In addition, the dithering helped us to clean cosmic rays and avoid gaps between the CCDs in the final images. The complete reduction process (including flat fielding, bias subtraction and bad–column elimination) yielded a final coadded image where the variation

of the sky was lower than 0.4% in the whole frame. Another effect associated with the wide field frames is the distortion of the field. In order to match the photometry of several filters, a good astrometric solution is needed to take into account these distortions. Using the *imcoords* IRAF tasks and taking as a reference the USNO B1.0 catalog, we were able to find an accurate astrometric solution (rms $\sim 0.5''$) across the full frame. The photometric calibration was performed using Landolt standard fields obtained during the observation.

We finally identified galaxies in our $B_{\rm H}$ and $R_{\rm H}$ images and measured their magnitudes with the SExtractor package (Bertin & Arnouts 1996) and AUTOMAG procedure. In a few cases (e.g. close companion galaxies, galaxies close to defects of the CCD) the standard SExtractor photometric procedure failed. In these cases we computed magnitudes by hand. This method consists in assuming a galaxy profile of a typical elliptical galaxy and scaling it to the maximum observed value. The integration of this profile gives us an estimate of the magnitude. This method is similar to PSF photometry, but assumes a galaxy profile, more appropriate in this case.

We transformed all magnitudes into the Johnson–Cousins system (Johnson & Morgan 1953; Cousins 1976). We used $B = B_{\rm H} + 0.13$ and $R = R_{\rm H}$ as derived from the Harris filter characterization (http://www.ast.cam.ac.uk/~wfcsur/technical/photom/colours/) and assuming a $B - V \sim 1.0$ for E–type galaxies (Poggianti 1997). As a final step, we estimated and corrected the galactic extinction $A_B \sim 0.10$, $A_R \sim 0.06$ from Burstein & Heiles's (1982) reddening maps.

We estimated that our photometric sample is complete down to $R = 20.5$ (22.0) and $B = 22.0$ (23.0) for $S/N = 5$ (3) within the observed field.

We assigned magnitudes to all galaxies of our spectroscopic catalog. We measured redshifts for galaxies down to magnitude $R \sim 20$, but a high level of completeness is reached only for galaxies with magnitude $R < 19$ (~45% completeness).

Table 1 lists the velocity catalog (see also Fig. 2): identification number of each galaxy, ID (Col. 1); right ascension and declination, α and δ (J2000, Col. 2); B and R magnitudes (Cols. 3 and 4); heliocentric radial velocities, $v = cz_\odot$ (Col. 5) with errors, Δv (Col. 6); redshift source (Col. 7; T:TNG, S:SDSS); member assignment (Col. 8; 1:A1240, 2:A1237, 0:background/foreground).

Table 1. Velocity catalog of 145 spectroscopically measured galaxies in the field of the A1237+A1240 complex. In Col. 1, IDs 75, 56, 111, 29 and 27 (in boldface) highlight BCGS, BCGN, BCGE, BCG1 and BCG2, respectively (see text). Asterisks in Col. 8 highlight emission line galaxies.

ID	α, δ (J2000)	B	R	v (km s^{-1})	Δv	So.	Cl.
1	11 22 00.12, +42 54 25.2	17.76	15.75	23230	53	S	0
2	11 22 03.36, +43 11 41.6	18.53	18.25	180587	338	S	0
3	11 22 04.44, +43 01 35.4	18.57	16.87	37090	40	S	0
4	11 22 24.24, +42 53 08.9	18.66	17.46	44576	27	S	0
5	11 22 41.52, +43 00 41.4	18.47	17.17	21546	49	S	0
6	11 22 46.20, +42 57 37.4	19.28	17.28	33915	46	S	0
7	11 22 59.88, +43 06 43.6	18.48	17.10	34993	32	S	0
8	11 23 08.52, +43 10 41.9	18.93	17.18	26827	42	S	0
9	11 23 09.24, +42 55 38.3	19.10	17.39	58448	31	S	2
10	11 23 10.32, +42 53 06.2	18.49	17.10	33987	41	S	0
11	11 23 11.96, +42 56 08.7	20.40	19.20	58737	78	T	∗2
12	11 23 14.37, +42 57 28.6	21.00	19.34	90603	72	T	∗0
13	11 23 15.00, +43 12 08.6	19.24	17.56	24005	30	S	0
14	11 23 15.76, +42 58 06.7	23.01	21.11	56786	150	T	2
15	11 23 16.45, +42 53 50.3	20.20	18.05	57516	56	T	2
16	11 23 18.74, +42 57 30.1	20.38	18.68	73676	88	T	∗0
17	11 23 19.68, +43 18 44.6	21.96	18.84	133977	49	S	0
18	11 23 20.92, +42 56 28.3	21.40	19.08	57994	100	T	2
19	11 23 21.02, +42 57 12.5	19.58	17.91	57551	72	T	2
20	11 23 21.69, +42 55 25.9	20.22	17.83	57982	52	T	2
21	11 23 22.07, +42 54 58.6	21.64	19.22	59445	92	T	2
22	11 23 22.07, +43 04 44.2	20.81	18.64	59551	83	T	1
23	11 23 23.23, +42 54 27.7	21.22	19.03	58431	82	T	2
24	11 23 23.70, +42 56 13.9	20.29	17.88	58813	38	T	2
25	11 23 23.88, +42 58 25.7	23.49	19.78	90451	142	T	∗0
26	11 23 24.26, +43 09 38.1	20.57	18.12	59406	140	T	1
27	11 23 24.64, +42 56 06.0	19.46	16.92	57965	38	T + S	2
28	11 23 25.78, +42 51 34.7	22.14	20.45	58742	120	T	2
29	11 23 25.80, +42 54 17.6	19.04	16.49	57482	52	S	2
30	11 23 26.04, +43 05 10.5	20.18	17.86	59031	50	T	1
31	11 23 27.35, +43 00 00.9	20.28	18.34	35290	70	T	0
32	11 23 27.80, +42 59 35.0	18.51	17.22	17883	26	T + S	∗0
33	11 23 28.33, +43 05 48.1	21.23	19.27	57149	174	T	1
34	11 23 28.35, +42 53 49.1	20.77	18.52	57489	36	T	2
35	11 23 28.43, +43 05 29.9	20.49	18.22	57988	61	T	1

3. Analysis and Results

3.1. Member selection

To select cluster members out of 145 galaxies having redshifts, we follow a two steps procedure. First, we perform the 1D adaptive–kernel method (hereafter DEDICA, Pisani 1993 and 1996; see also Fadda et al. 1996; Girardi et al. 1996). We search for significant peaks in the velocity distribution at >99% c.l.. This procedure detects A1237+A1240 as a peak at $z \sim 0.196$ populated by 95 galaxies considered as candidate cluster members (see Fig. 3). Out of 50 non members, 24 and 26 are foreground and background galaxies, respectively.

All the galaxies assigned to the cluster peak are analyzed in the second step which uses the combination of position and velocity information: the "shifting gapper" method by Fadda et al. (1996). This procedure rejects galaxies that are too far in velocity from the main body of galaxies within a fixed bin that shifts along the distance from the cluster center. The procedure is iterated until the number of cluster members converges to a stable value. Following Fadda et al. (1996) we use a gap of 1000 km s^{-1} – in the cluster rest–frame – and a bin of 0.6 h_{70}^{-1} Mpc, or large enough to include 15 galaxies.

The choice of the center of A1240 is not obvious. No evident dominant galaxy is present, rather there are some luminous galaxies. In particular, the two brightest ones, ID. 75 and ID. 56, lie in the southern and northern region of A1240, respectively, and show comparable luminosity (hereafter BCGS and BCGN). The third one is located in the eastern region, but is $\gtrsim 0.5$ R–magnitudes fainter than BCGS and BCGN (ID. 111, hereafter BCGE). As for the cluster center, hereafter we assume the position of the centroid of the X–ray emission as recovered by David et al. (1999) [R.A.=$11^{\rm h}23^{\rm m}37\overset{\rm s}{.}6$, Dec.=+43°05′51″ (J2000.0)] which lies between the two dominant galaxies. After the "shifting gapper" procedure we obtain a sample of 89 fiducial cluster members (see Fig. 4).

We also check the result of alternative member selection procedures. We apply the "shifting gapper" procedure adopting as

Table 1. Continued.

ID	α, δ (J2000)	B	R	v (km s^{-1})	Δv	So.	Cl.
36	11 23 28.81, +42 52 09.7	21.81	20.33	56626	86	T	2
37	11 23 29.80, +42 53 31.6	21.82	19.72	58741	54	T	2
38	11 23 29.97, +42 57 51.3	19.90	17.63	58621	142	T	2
39	11 23 30.13, +43 06 58.6	21.41	18.79	97901	128	T	0
40	11 23 30.17, +43 02 18.2	20.45	18.67	57717	112	T	1
41	11 23 30.84, +42 54 55.8	19.71	17.30	57368	43	S	2
42	11 23 31.07, +42 59 27.6	21.74	19.63	102577	106	T	0
43	11 23 31.17, +42 53 53.3	19.30	18.16	44948	88	T	$*0$
44	11 23 31.20, +42 54 45.8	19.84	17.54	59205	60	T	2
45	11 23 31.32, +42 54 26.3	21.30	19.31	59217	84	T	2
46	11 23 32.10, +43 08 42.0	20.75	18.41	57592	81	T	1
47	11 23 32.40, +43 09 06.8	22.03	19.59	58446	76	T	1
48	11 23 32.68, +43 07 56.0	20.83	18.79	58949	148	T	1
49	11 23 32.75, +42 57 31.8	19.75	17.60	57246	68	T	2
50	11 23 33.08, +43 06 32.2	20.18	17.86	59329	150	T	1
51	11 23 33.72, +43 14 47.4	19.67	17.25	59070	49	S	1
52	11 23 33.84, +43 08 53.3	20.96	18.62	84868	112	T	$*0$
53	11 23 34.15, +43 08 12.9	20.35	18.07	57839	128	T	1
54	11 23 34.67, +43 04 12.1	20.50	18.24	58620	64	T	1
55	11 23 34.82, +43 01 56.9	20.14	19.22	23909	87	T	$*0$
56	11 23 35.26, +43 08 31.7	18.74	16.22	58353	96	T	1
57	11 23 35.46, +43 04 57.7	19.57	16.97	58717	46	T + S	1
58	11 23 35.48, +43 05 13.7	19.84	17.23	58230	100	T	1
59	11 23 35.52, +42 53 43.8	19.23	17.46	58805	43	S	2
60	11 23 35.60, +43 05 06.1	20.79	18.93	58415	180	T	1
61	11 23 35.77, +43 11 19.2	20.99	18.80	88635	156	T	$*0$
62	11 23 36.00, +43 16 06.3	21.02	18.99	53996	94	T	0
63	11 23 36.34, +43 07 11.1	20.99	18.77	58358	204	T	1
64	11 23 36.56, +42 57 20.5	19.67	17.58	56715	78	T	2
65	11 23 36.68, +43 09 01.9	20.38	18.00	60953	116	T	0
66	11 23 36.77, +42 59 13.5	21.03	18.88	57097	84	T	2
67	11 23 36.77, +43 11 44.5	20.99	19.00	59749	92	T	1
68	11 23 36.88, +43 04 56.3	22.13	19.75	59656	192	T	1
69	11 23 36.91, +43 15 37.3	22.17	20.82	153440	130	T	$*0$
70	11 23 37.16, +42 53 46.7	20.28	18.81	56870	74	T	$*2$

Table 1. Continued.

ID	α, δ (J2000)	B	R	v (km s^{-1})	Δv	So.	Cl.
71	11 23 37.17, +43 11 31.4	20.36	18.15	58635	142	T	1
72	11 23 37.28, +43 01 16.6	21.38	19.31	59878	70	T	1
73	11 23 37.34, +43 09 10.2	21.47	19.01	100284	258	T	0
74	11 23 37.53, +43 04 19.9	21.90	19.79	57709	118	T	1
75	11 23 37.69, +43 03 28.2	18.82	16.12	58817	54	T	1
76	11 23 37.83, +43 03 10.8	19.76	17.11	56550	78	T	1
77	11 23 38.13, +43 09 43.9	20.84	19.42	60307	194	T	$*1$
78	11 23 38.22, +43 03 38.6	20.23	18.01	59542	92	T	1
79	11 23 38.32, +43 09 39.9	21.24	19.26	58342	140	T	1
80	11 23 38.35, +43 07 42.0	20.78	18.53	57397	53	T	1
81	11 23 38.37, +43 09 55.0	20.80	19.91	59828	148	T	1
82	11 23 38.46, +43 07 48.2	20.90	19.57	58605	200	T	1
83	11 23 38.63, +43 01 49.1	21.23	18.87	58509	80	T	1
84	11 23 38.85, +43 04 36.8	20.57	19.33	55562	134	T	$*1$
85	11 23 39.15, +43 02 35.5	20.77	18.73	57478	78	T	1
86	11 23 39.54, +43 10 07.4	22.07	19.63	58711	146	T	1
87	11 23 40.08, +43 10 36.4	20.74	18.37	57351	160	T	1
88	11 23 40.47, +43 09 18.7	21.41	18.97	59078	94	T	1
89	11 23 40.50, +43 02 59.3	20.92	18.79	56851	82	T	1
90	11 23 40.87, +42 53 37.4	17.00	15.19	23141	37	T + S	0
91	11 23 41.42, +42 52 33.5	20.59	19.47	58938	118	T	$*2$
92	11 23 41.92, +43 10 51.7	19.76	17.41	57628	138	T	1
93	11 23 42.04, +43 01 03.9	21.19	19.61	56216	120	T	1
94	11 23 42.05, +43 12 17.8	19.45	17.16	57828	42	T + S	1
95	11 23 42.60, +43 15 17.3	20.91	18.65	59502	120	T	1
96	11 23 42.85, +43 09 29.3	22.03	19.57	57407	144	T	1
97	11 23 42.89, +43 12 24.4	21.43	18.91	90672	92	T	0
98	11 23 42.94, +42 56 16.2	18.87	17.55	23440	94	T	$*0$
99	11 23 43.03, +43 10 09.4	21.59	19.79	90196	186	T	0
100	11 23 44.16, +43 17 44.5	18.97	17.96	59099	29	S	1
101	11 23 44.19, +42 53 30.4	21.03	18.45	57649	46	T	2
102	11 23 44.90, +43 14 02.4	21.25	19.06	59238	186	T	1
103	11 23 45.26, +43 08 14.8	21.35	19.93	56860	110	T	1
104	11 23 45.29, +43 12 38.4	21.18	18.88	98761	94	T	0
105	11 23 46.58, +42 59 57.6	20.57	18.78	56478	76	T	1

cluster center the brightest cluster galaxy (BCGS). We find a cluster sample of 89 galaxies, 88 of which are in common with our above sample. In order to analyze the effect of a fully alternative selection procedure we also apply the classical 3–σ clipping procedure by Yahil & Vidal (1977) on the whole sample of 145 galaxies after a very rough cut in the velocity space, i.e. rejecting galaxies with velocities differing by more than 8000 km s^{-1} from the mean velocity. This classical procedure leads to a sample of 90 galaxies, 89 of which forms our adopted sample. In conclusion, the sample of member galaxies we adopt in this work is quite robust against the member selection procedure.

The galaxy distribution analyzed through the 2D DEDICA method clearly shows the presence of a southern external clump (see Fig. 5, see also Sect. 3.7). Gal et al. (2003) recovered a cluster in the same position from the digitized Second Palomar Observatory Sky Survey. We identify this galaxy clump with A1237 which is likely to have a cluster redshift similar to that of A1240 (cf. the magnitudes of their 10th–ranked cluster galaxies, Abell et al. 1989). Notice that the center reported by Abell et al. is quite imprecise and lies on the southern border of the galaxy concentration we detect.

We use the 2D DEDICA results, i.e. the peaks detected in the 2D galaxy distribution, to assign galaxies to different subclumps. The 2D DEDICA algorithm detects nine peaks, four of which are more significant than the 99% c.l.. The southern three peaks, only one of which is very significant, are assigned to A1237 (for a total of 27 members). The six northern peaks, three of which are very significant, are assigned to A1240 (for a total of 62 members). This assignment is shown in Fig. 6 – left panel.

As for A1240, the 2D DEDICA algorithm shows a clear bimodal structure (see Fig. 5) along the North-South direction. This bimodality is also shown in our analysis of photometric "likely" members in Sect. 3.7 and corresponds to the elongated hot gas distribution shown by the previous analyses of ROSAT data (David et al. 1999; Bonafede et al. 2009) and our analysis of Chandra data (see Sect. 4). Therefore we decide to consider: a southern structure – hereafter A1240S – associated to the southern peak of A1240 (the most significant in the whole DEDICA analysis); a northern structure – hereafter a1240N – associated to the four northern peaks (two of which are very significant). In this way we assign 32 (27) members to A1240N (A1240S). A1240S and A1240N host the brightest and the second bright-

Table 1. Continued.

ID	α, δ (J2000)	B	R	v (km s^{-1})	Δv	So.	Cl.
106	11 23 48.35, +43 11 11.6	20.54	18.95	58801	84	T	∗1
107	11 23 49.20, +43 08 07.9	20.39	18.30	57904	118	T	1
108	11 23 49.42, +43 00 17.4	21.08	18.78	58494	116	T	1
109	11 23 49.54, +43 07 59.1	22.51	20.07	84937	196	T	0
110	11 23 49.83, +43 03 52.8	21.37	18.79	91883	118	T	0
111	11 23 49.92, +43 05 44.7	19.21	16.72	56134	66	T	1
112	11 23 50.86, +43 13 22.2	21.25	19.06	59144	104	T	1
113	11 23 51.09, +43 12 01.0	21.51	19.94	61506	118	T	0
114	11 23 51.14, +43 00 09.2	20.62	19.24	48223	126	T	∗0
115	11 23 51.15, +43 12 06.5	20.98	19.59	78030	138	T	∗0
116	11 23 51.87, +43 11 54.8	20.96	18.85	152164	138	T	0
117	11 23 52.35, +43 12 45.5	21.11	19.50	55225	94	T	0
118	11 23 52.44, +42 54 36.4	18.55	17.45	23511	28	S	0
119	11 23 52.44, +43 03 28.1	19.62	17.15	58336	48	S	1
120	11 23 52.47, +42 58 19.6	21.25	19.12	58639	86	T	1
121	11 23 52.51, +43 14 50.0	20.93	18.83	59284	104	T	1
122	11 23 52.59, +43 06 05.3	22.05	19.03	84545	166	T	0
123	11 23 53.52, +43 06 13.3	19.76	17.30	59022	47	S	1
124	11 23 54.07, +43 15 07.2	20.21	18.63	21528	86	T	0
125	11 23 54.10, +43 11 24.4	20.63	18.97	77906	94	T	∗0
126	11 23 54.21, +43 14 17.2	21.87	19.94	106774	98	T	0
127	11 23 54.31, +42 58 28.1	20.48	18.59	87022	90	T	0
128	11 23 54.60, +43 04 30.0	17.76	16.07	21275	45	S	0
129	11 23 55.13, +43 14 26.0	19.61	18.90	24046	30	T	∗0
130	11 23 56.24, +42 59 40.4	19.98	17.58	58805	68	T	1
131	11 23 56.76, +42 58 06.2	18.00	16.57	23303	31	S	0
132	11 23 57.23, +43 09 56.6	21.71	20.56	58966	130	T	∗1
133	11 23 57.48, +43 13 13.8	21.14	18.78	331328	450	S	0
134	11 23 57.57, +43 13 01.2	19.36	17.22	54792	80	T	0
135	11 23 57.81, +43 10 41.5	21.44	19.24	58346	156	T	1
136	11 24 01.38, +42 58 55.5	20.18	18.45	48099	74	T	0
137	11 24 01.72, +43 15 50.5	21.28	20.33	78070	71	T	∗0
138	11 24 01.75, +43 00 42.0	21.17	19.56	57426	144	T	∗1
139	11 24 01.80, +43 08 57.5	17.77	16.31	21326	56	S	0
140	11 24 02.20, +43 02 44.4	22.03	19.78	56604	212	T	1
141	11 24 03.24, +43 13 30.7	19.66	18.04	96076	37	S	0
142	11 24 03.60, +42 56 11.4	19.51	17.03	58204	46	S	1
143	11 24 04.83, +43 13 48.0	17.54	15.48	21158	112	T	0
144	11 24 07.19, +43 13 32.7	20.41	18.03	55467	102	T	0
145	11 24 31.68, +42 56 49.6	21.16	18.28	92075	75	S	0

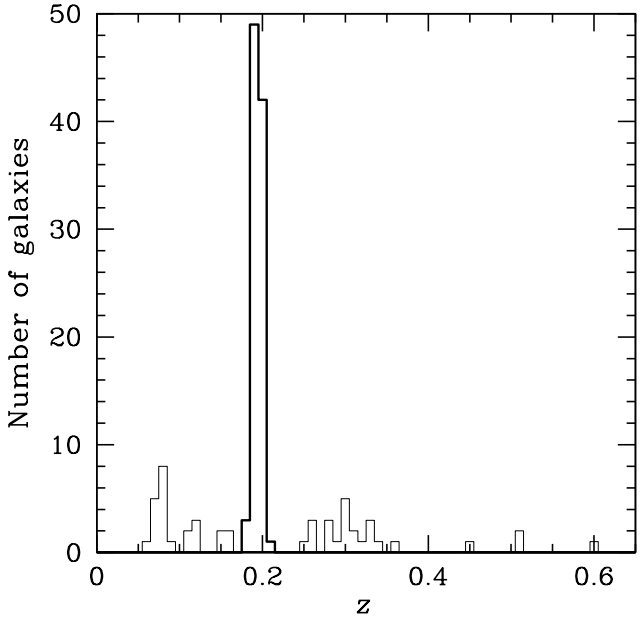

Fig. 3. Redshift galaxy distribution. The solid line histogram refers to the 95 galaxies assigned to the A1237+A1240 complex according to the DEDICA reconstruction method.

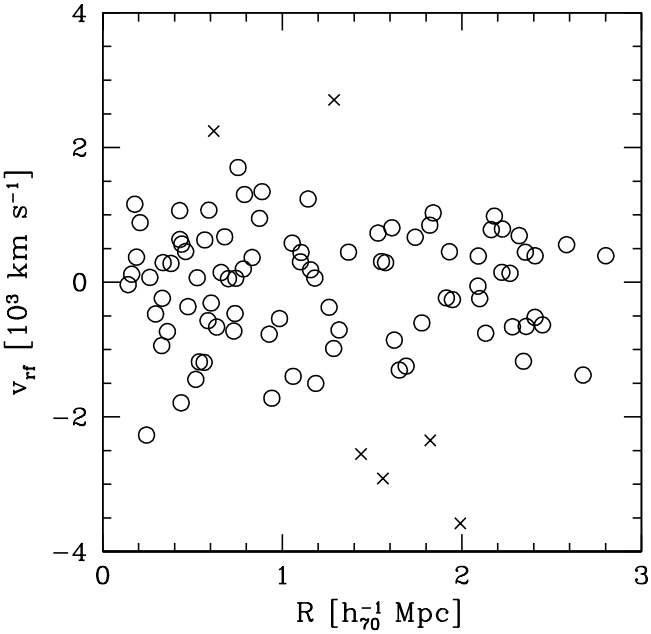

Fig. 4. Rest–frame velocity vs. projected clustercentric distance for the 95 galaxies in the main peak (Fig. 3) showing galaxies detected as interlopers by our "shifting gapper" procedure (crosses). Circles indicate the 89 cluster members.

est galaxies, BCGS and BCGN, respectively. We consider separately three galaxies belonging to a minor, eastern peak (hereafter A1240E) since their assignation to A1240N or A1240S is not obvious. A1240E hosts the BCGE. The assignment of galaxies within A1240 is summarized as follow: we assign to A1240S the galaxies belonging to the southern peak (detected with a > 99.99% c.l.); to A1240N the galaxies belonging to the four, northern peaks (two of which are detected with a > 99.8% c.l.); to a1240E the galaxies belonging to the eastern peak.

3.2. The A1237+A1240 complex in the velocity space

According to the 1D Kolmogorov–Smirnov test (hereafter 1DKS–test; see, e.g., Press et al 1992), there is no significant difference between the velocity distributions of A1237 and A1240 (see also Fig. 6 – right panel). This result suggests us to investigate the global velocity distribution of the complex.

We analyze the velocity distribution of cluster galaxies (see Fig. 7) using a few tests where the null hypothesis is that the velocity distribution is a single Gaussian. We estimate three shape estimators: the kurtosis, the skewness, and the scaled tail index (see, e.g., Beers et al. 1991). According to the value of the skewness (-0.379) the velocity distribution is marginally asymmetric

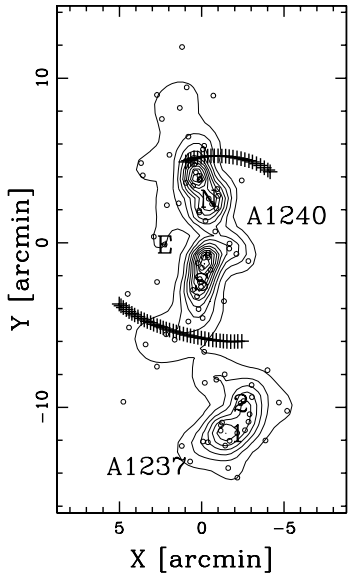

Fig. 5. Spatial distribution on the sky and relative isodensity contour map of cluster members (A1237+A1240), obtained with the DEDICA method. The positions of the brightest galaxies are indicated (BCGN, BCGS, BCGE for A1240 and BCG1 and BCG2 for A1237). The plot is centered on the cluster center defined in this paper as the X–ray center. The two relics are indicated in a schematic way.

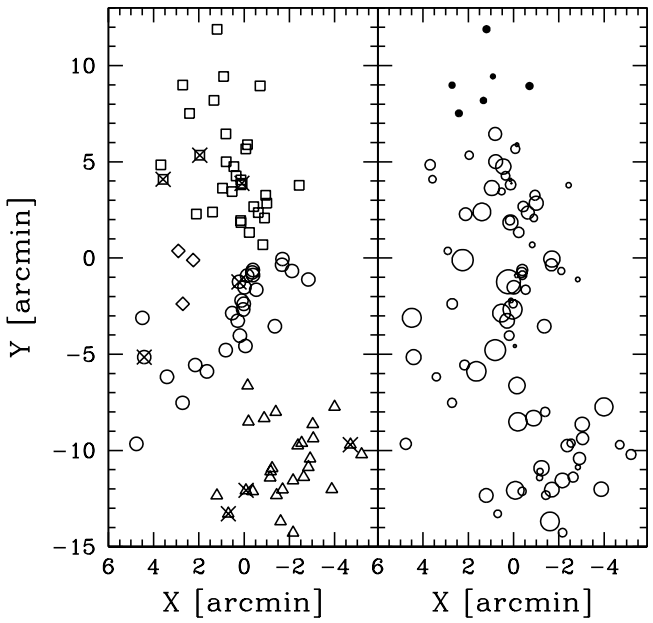

Fig. 6. Spatial distribution on the sky of 89 cluster members. *Left panel*: open symbols indicate cluster members. In particular, squares, circles, rotated squares and triangles indicate A1240N, A1240S, A1240E and A1237. The crosses indicate emission line galaxies. *Right panel*: the larger the symbol, the smaller is the radial velocity. The six close northern circles indicate the high velocity galaxies we consider responsible of the apparent large global mean velocity of A1240N galaxies (see Sect. 3.4 and Fig. 10 in the following, too).

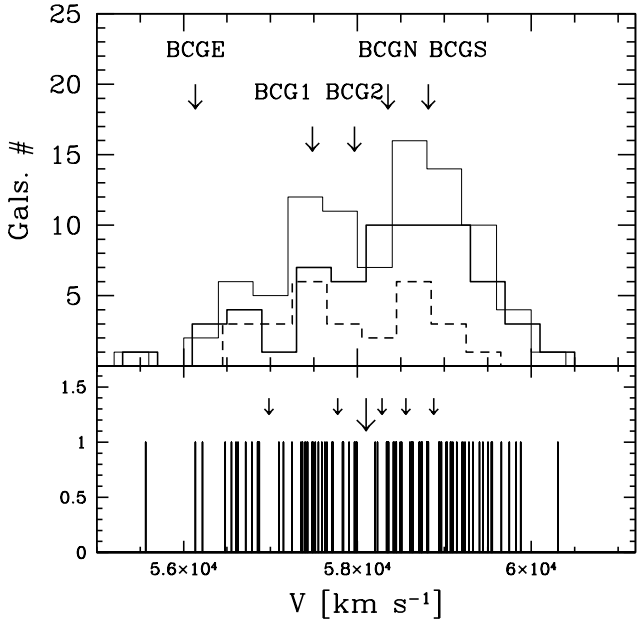

Fig. 7. *Upper panel*: velocity histogram for the whole cluster sample (thin line), A1240 (solid line) and A1237 (dashed line). The velocities of the three brightest galaxies of A1240 are indicated (BCGN, BCGS and BCGE), as well as the two brightest galaxies of A1237 (BCG1 and BCG2). *Lower panel*: stripe density plot where the arrows indicate the positions of the significant gaps. The main and minor weighted gaps are indicated by big and small arrows, respectively.

differing from a Gaussian at the 90−95% c.l. (see Table 2 of Bird & Beers 1993). We also analyze the presence of "weighted gaps" in the velocity distribution. A weighted gap in the space of the ordered velocities is defined as the difference between two contiguous velocities, weighted by the location of these velocities with respect to the middle of the data (Wainer and Schacht 1978; Beers et al. 1991). We detect a strongly significant gap (at the > 99.9% c.l.) and five minor gaps (at the $\gtrsim$ 98% c.l.), see Fig. 7 – lower panel. The most important gap, very significant since it is located in the central region of the velocity distribution, separates the cluster into two subgroups of 37 and 52 galaxies. When comparing the 2D galaxy distributions of these subgroups we find no difference according to the 2D Kolmogorov–Smirnov test (Fasano & Franceschini 1987).

We also perform the 2D and 3D Kaye's mixture model (KMM) test (as implemented by Ashman et al. 1994) and compare the results to check the effect of the addition of the velocity information. The KMM algorithm fits a user–specified number of Gaussian distributions to a dataset and assesses the improvement of that fit over a single Gaussian and give an assignment of objects into groups. We use the A1237+A1240 galaxy assignment found by the 2D DEDICA analysis to determine the first guess when fitting two groups. The 2D KMM algorithm fits a two–group partition, at the > 99.9% c.l. according to the likelihood ratio test, leading to two groups of 66 and 23 galaxies. The addition of the velocity information in the KMM algorithm leads to the same group partition.

Finally, we combine galaxy velocity and position information to compute the Δ–statistics devised by Dressler & Shectman (1988). This test is sensitive to spatially compact subsystems that

have either an average velocity that differs from the cluster mean, or a velocity dispersion that differs from the global one, or both. We find no significant substructure.

We conclude that, although the velocity distribution shows evidence of a complex structure, A1237 and A1240 are so similar in the velocity space that the velocity information is not useful to improve the galaxy assignment recovered from the 2D analysis (see Sect. 3.1).

3.3. Global Kinematical properties

As for the whole cluster complex, by applying the biweight estimator to the 89 members (Beers et al. 1990), we compute a mean redshift of $\langle z \rangle = 0.1937 \pm 0.0003$, i.e. $\langle v \rangle = (58273 \pm 89)$ km s^{-1}. We estimate the LOS velocity dispersion, σ_V, by using the biweight estimator and applying the cosmological correction and the standard correction for velocity errors (Danese et al. 1980). We obtain $\sigma_V = 842^{+63}_{-55}$ km s^{-1}, where errors are estimated through a bootstrap technique.

The results obtained for the 62 members of A1240 are: $\langle z \rangle = 0.1948 \pm 0.0004$, i.e. $\langle v \rangle = (58408 \pm 111)$ km s^{-1} , and $\sigma_V = 870^{+91}_{-79}$ km s^{-1}. To evaluate the robustness of σ_V of A1240 we analyze the velocity dispersion profile (Fig. 8). The integral profile is roughly flat in the external cluster regions suggesting that the value of σ_V for A1240 is quite robust. Figure 8 also shows that the $\langle v \rangle$ and σ_V profiles are not disturbed by the presence of A1237.

Table 2 lists the number of the member galaxies N_g and the main kinematical properties of A1237 and A1240.

Figure 9 compares the $\langle v \rangle$ and σ_V profiles of A1240 and A1237, where for A1240 we show separately the results for A1240N and A1240S. The value $\langle v \rangle$ of A1237 is similar to that of A1240S, suggesting a continuity in the velocity field. However the value of σ_V of A1237 is clearly lower than that of A1240S, suggesting that A1237 is really a less massive system.

3.4. Internal structure of A1240

According to the 1DKS–test there is no difference between the velocity distributions of A1240N and A1240S. The velocity distribution of A1240 shows signatures of non–Gaussianity similar to those of the whole cluster complex (e.g. a slight asymmetry and an important gap, see Fig. 7). Like for the A1237 vs. A1240 case, we find that A1240N and A1240S are so similar in the velocity space that the velocity information is not useful to improve the galaxy assignment. However, at the contrary of the A1237 vs. A1240 case, A1240N and A1240S are spatially closer and likely strongly interacting (see Sect. 5). This suggests that the galaxy assignment might be questionable and that we must devote more cure in determining the individual kinematical properties of the two subclumps.

The value of global $\langle v \rangle$ of A1240N is nominally larger than that of A1240S, i.e. $\langle v \rangle = (58624 \pm 128)$ km s^{-1} and $\langle v \rangle = (58091 \pm 195)$ km s^{-1} respectively, only at a $\sim 2\sigma$ c.l. Moreover, looking at Fig. 9, the two cores of A1240N and A1240S seem to have similar $\langle v \rangle$: this is better shown in Fig.10, where we directly compare the profiles of A1240N and A1240S. The large global $\langle v \rangle$ of A1240N is likely due to few high velocity galaxies in the extreme northern cluster regions (see the six galaxies shown as close circles in Fig. 6 – right panel; see also Fig. 10). Indeed, the recent merger of two subclumps may result in a plume, or arm, of outflying galaxies detected for their different velocity with respect to the cluster (see e.g. the case of Abell 3266; Quintana et al. 1999 and Flores et al. 2000). Due to these difficulties in detecting a quantitative difference between A1240N and A1240S, we prefer to use the position and velocity of BCGN and BCGS as tracers of the two interveining clumps. In fact, dominant galaxies trace the cluster substructures (Beers & Geller 1983) and are good tracers of interacting subclumps during a cluster merger, too (e.g., Boschin et al. 2006; Barrena et al. 2007a; Boschin et al. 2009).

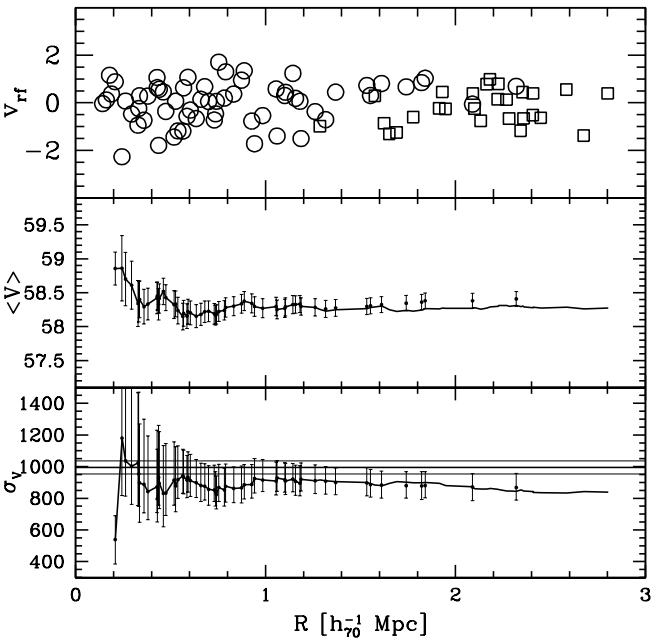

Fig. 8. *Upper panel*: rest–frame velocity (in units of 10^3 km s^{-1}) vs. projected clustercentric distance for the 89 cluster galaxies. Circles and squares indicate members of A1240 and A1237. Central and lower panels: integral profiles of mean LOS velocity (in units of 10^3 km s^{-1}) and LOS velocity dispersion (in units of km s^{-1}) for the 62 members of A1240 (dots with the 68% c.l. errorbar) and for all the 89 cluster members (A1237+A1240, solid line). The mean and dispersion at a given (projected) radius from the cluster–center is estimated by considering all galaxies within that radius – the first value computed on the five galaxies closest to the center. In the lower panel, the horizontal lines represent the X–ray temperature with the respective 68% errors transformed in σ_V assuming the density–energy equipartition between gas and galaxies, i.e. $\beta_{spec} = 1$ where $\beta_{spec} = \sigma_V^2/(kT/\mu m_p)$ with $\mu = 0.58$ the mean molecular weight and m_p the proton mass. In all the panels the center is the X–ray center of A1240.

The nominal value of global σ_V of A1240N is smaller than that of A1240S, $\sigma_V = 709^{+88}_{-83}$ km s^{-1} and $\sigma_V = 991^{+149}_{-99}$ km s^{-1} respectively. Using the brightest galaxies as centers the comparison of the respective σ_V profiles confirms this trend (see Fig.10 – right lower panel). Thus, although the nominal values of individual σ_V might be not fully reliable, we decide to adopt them for describing A1240N and A1240S.

Table 2 summarizes the properties of A1240N and A1240S.

3.5. Internal structure of A1237

As for A1237, it appears dominated by two bright galaxies, BCG1 and BCG2 (IDs. 29 and 27, see Table 1) and the 2D DEDICA algorithm shows the presence of one significant peak

Table 2. Global properties of galaxy systems.

System	N_g	α, δ (J2000)	$< v >$ km s^{-1}	σ_V km s^{-1}	R_{vir} h_{70}^{-1}Mpc	$M(< R_{vir})$ $h_{70}^{-1} 10^{14} M_\odot$
A1237	27	112329.5 + 425419	58021 ± 145	738^{+82}_{-54}	1.6	6 ± 2
A1240	62	112337.6 + 430551	58408 ± 111	870^{+91}_{-79}	1.9 – 2.4[b]	9 – 19[b]
A1240N[a]	32	112335.2 + 430832	~ 58353	709^{+88}_{-83}	1.6	5 ± 2
A1240S[a]	27	112337.7 + 430328	~ 58817	991^{+149}_{-99}	2.2	14 ± 5

[a] **As center and mean velocity of this clump we list the position and velocity** of the respective brightest galaxy.
[b] The lower limit comes from the observed σ_V. The upper limit is obtained when considering the bimodal structure of the cluster (see text).

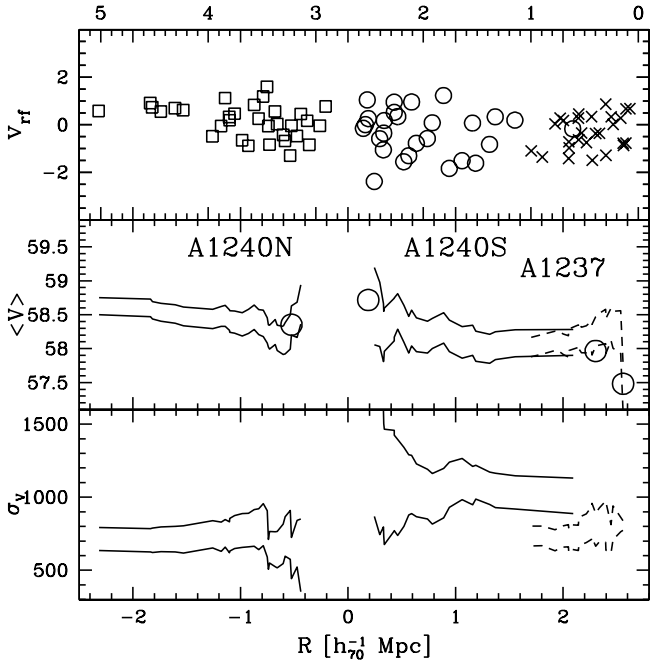

Fig. 9. *Upper panel*: rest–frame velocity (in units of 10^3 km s^{-1}) vs. projected clustercentric distance for the members of A1240N (squares), A1240S (circles) and A1237 (crosses). In this and other panels the lower axis give the clustercentric distance of A1240N (A1240S) galaxies versus the negative (positive) axis from the A1240 center, while the upper axis give the clustercentric distance of A1237 galaxies from the A1237 center. The center of A1240 is defined as the X–ray center. The center of A1237 is defined as the position of the main peak in the 2D analysis. *Central and lower panels*: 68% error bands of integral profiles of LOS mean velocity (in units of 10^3 km s^{-1}) and LOS velocity dispersion (in units of km s^{-1}) for A1240N and A1240S (solid lines) and A1237 (dashed lines). The circles in the *central panel* indicate the positions and velocities of the two brightest galaxies of A1240 (BCGN and BCGS) and the two brightest galaxies of A1237 (BCG1 and BCG2).

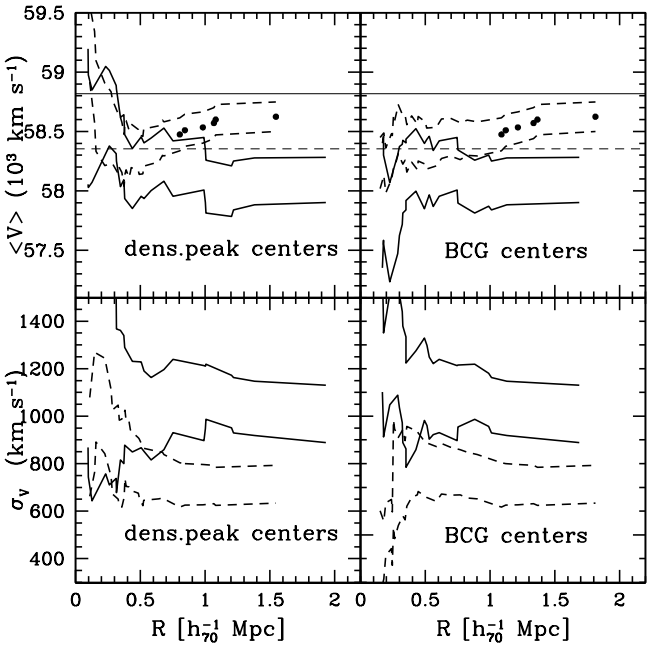

Fig. 10. *Upper panels*: Error bands of integral profiles of LOS mean velocity for A1240N (dashed line) and A1240S (solid line). The distance is computed using as the center the position of the most important peak (on the left) and the position of the brightest cluster member (on the right). The horizontal lines indicate the velocities of BCGN and BCGS (dashed and solid lines, respectively). The close circles point out at which radius the six northern high velocity galaxies in A1240N are included to show their effect on the estimate of the mean velocity (see the text and Fig. 6, too). *Lower panels*: The same for integral profiles of the LOS velocity dispersion.

(at the > 99% c.l.) and two minor peaks significant at the 97% and 89% c.l. (see the somewhat elongated structure of A1237 in Fig. 5). Both the analysis of SDSS and our photometric data show that A1237 has only one well defined peak in the 2D galaxy distribution (see Sect. 3.7). This last result is based on a much larger sample, thus we conclude that we have no evidence for a complex structure in A1237. The velocity distribution shows evidence for a platykurtic behavior, but at a poorly significant level (at the ~ 95% c.l.).

3.6. Mass estimates

Under the usual assumptions (cluster sphericity, dynamical equilibrium and galaxy distribution tracing the mass distribution), we can compute global virial quantities. Following the prescriptions of Girardi & Mezzetti (2001), the virial radius is $R_{vir} = 0.17 \times \sigma_V / H(z)\ h_{70}^{-1}$ Mpc (see their Eq. 1 after introducing the scaling with $H(z)$; see also Eq. 8 of Carlberg et al. 1997 for

R_{200}) and the virial mass (Limber & Mathews 1960; see also, e.g., Girardi et al. 1998) is:

$$M = 3\pi/2 \cdot \sigma_V^2 R_{PV}/G - \mathrm{SPT}. \quad (1)$$

The quantity SPT, the surface pressure term correction (The & White 1986), is assumed to be equal to the 20% of the mass since this is the typical value recovered for the mass computed within the virial radius in the literature when the data of many clusters are combined together to enlarge the statistics (Carlberg et al. 1997; Girardi et al. 1998). The quantity R_{PV} is a projected radius (equal to two times the projected harmonic radius). The value of R_{PV} depends on the size of the sampled region and possibly on the quality of the spatial sampling (e.g., whether the cluster is uniformly sampled or not). It is also possible to use an alternative estimate of R_{PV} based on a priori knowledge of the galaxy distribution (see the Appendix in Girardi et al. 1995). Following Girardi et al. (1998; see also Girardi & Mezzetti 2001) we can assume a King–like distribution with parameters typical of nearby/medium–redshift clusters: a core radius $R_c = 1/20 \times R_{vir}$ and a slope–parameter $\beta_{fit,gal} = 0.8$, i.e., the volume galaxy density at large radii scales as $r^{-3\beta_{fit,gal}} = r^{-2.4}$. With these assumptions we can use the eq. A6 of Girardi et al. (1995) to estimate R_{PV}, see also eq. 13 of Girardi et al. 1998 for a useful approximation (i.e., $R_{PV} = 1.189 R_{vir}[1+0.053(R_{vir}/R_c)]/[1+0.117(R_{vir}/R_c)]$. Having assumed the galaxy distribution, the value of R_{PV} depends only on R_{vir}. In this way our estimates of global virial quantities only depend on our estimate of σ_V.

Through this procedure we obtain a mass estimate $M_{A1237}(< R_{vir} = 1.63\ h_{70}^{-1}\mathrm{Mpc}) = (6 \pm 2) \times 10^{14}\ h_{70}^{-1}\ M_\odot$ and $M_{A1240}(< R_{vir} = 1.92\ h_{70}^{-1}\mathrm{Mpc}) = (9 \pm 3) \times 10^{14}\ h_{70}^{-1}\ M_\odot$.

When a cluster shows a strongly substructured appearance (e.g., a bimodal structure), the use of the global σ_V to compute the mass might be misleading (Girardi et al. 1997 and refs. therein). The true mass could be overestimated or underestimated depending on the angle of view of the cluster structure. When the two subclumps are aligned along the LOS, they cannot be clearly distinguished in their projection onto the sky, but they can appear as two peaks (less or more overlapped, depending on their relative velocity) in the redshift distribution: in this case the mass estimated by the observed global σ_V is likely to be an overestimate of the true cluster mass (e.g., cf. Tabs. 7 and 8 of Girardi et al. 1998). When the two subclumps are aligned along an axis parallel to the plane of sky, they appear as two structures in their projection onto the sky but they cannot be distinguished in the redshift distribution (since their relative velocity has no component along the LOS direction). In this case the global velocity distribution is likely formed by the velocity distributions of the two clusters somewhat superimposed and the observed global σ_V does not take into account the existence of both the two subclumps.

The A1240N+A1240S system is comparable to the second case discussed above: the two subclumps are distinguished in the sky, but lie at a similar z. Indeed our analysis of Sect. 5 will show that the axis of the A1240N+A1240S system is likely roughly parallel to the plane of sky. A more reliable mass estimate of A1240 might be obtained adding the mass estimates of the two subclumps, each mass recovered from their respective σ_V (see Table 2). We obtain a mass $M_{A1240} \sim 1.9 \times 10^{15}\ h_{70}^{-1}\ M_\odot$. Another possible approach is to consider the future, virialized A1240 cluster and its global properties. Since the cluster virial mass computed within the virial radius scales with $\sim \sigma_V^3$, we expect that the $\sigma_{V,vir}$ of the virialized A1240 corresponds to $(\sigma^3_{V,A1240N} + \sigma^3_{V,A1240S})^{1/3}$, i.e. $\sigma_{V,vir} \sim 1100$ km s^{-1} well larger than the LOS σ_V measured on observed data. This corresponds to a mass of $M_{A1240}(< R_{vir} = 2.4\ h_{70}^{-1}\mathrm{Mpc}) \sim 1.9 \times 10^{15}\ h_{70}^{-1}\ M_\odot$ in good agreement with the above estimate.

In conclusion, we estimate a mass range of $M_{A1240} = (0.9 - 1.9) \times 10^{15}\ h_{70}^{-1}\ M_\odot$ and of $M_{A1237+A1240} = (1.5 - 2.5) \times 10^{15}\ h_{70}^{-1}\ M_\odot$.

3.7. Analysis of photometric data

The results of the 2D DEDICA method applied to the 89 cluster members are shown in Sect. 3.1. However, our spectroscopic data suffer from magnitude incompleteness and the field around the cluster is not covered in an homogeneous way. To overcome these limits we use our photometric catalog.

We select likely members on the basis of the B–R vs. R relation, as already performed in some previous works of ours (e.g., Barrena et al. 2007b). To determine the relation we fix the slope according to López–Cruz et al. (2004, see their Fig. 3) and apply the two–sigma–clipping fitting procedure to the cluster members obtaining B–$R = 3.557 - 0.069 \times R$ for the red sequence of A1240 galaxies. Figure 11 shows B–R vs. R diagram for galaxies with available spectroscopy and the fitted line.

Out of our photometric catalog we consider galaxies (objects with SExtractor stellar index ≤ 0.9) lying within 0.25 mag of the relation. Following Visvanathan & Sandage (1977) the width of 0.25 mag approximately corresponds to 2σ around the color–magnitude relation (see also Mazure et al. 1988 for a classical application to Coma cluster). The contour map for 370 likely cluster members having $R \leq 20.5$ shows the bimodal structure of A1240 and the presence of A1237, confirming the results of Sect. 3.1 (see Fig. 12). Similar results are obtained with different magnitude cut–offs (e.g., $R \leq 20$ and $R \leq 21$).

In this paper we also use public photometric data from the SDSS. In particular, we use r', i', z' magnitudes, already corrected for Galactic extinction and consider galaxies within a radius of 30′ from the cluster center.

Following Boschin et al. (2008, see also Goto et al. 2002), out of SDSS photometric catalog we consider galaxies (here objects with r' phototype parameter = 3) lying within ±0.08 mag from the median values of r'–i'=0.47 and i'–z'=0.32 colors of the spectroscopically cluster members. The value of 0.08 mag is two times the typical scatter reported by Goto et al. (2002) for the corresponding color–magnitude relations r'–i' vs. r' and i'–z' vs. r'. However, this member selection seems not enough conservative for the case of A1240. In fact, using our spectroscopic catalog, we notice that this color–color selection recognizes as "likely members" 21 out of the 56 non member galaxies (against the 11 out of 56 by using the color–magnitude selection). Therefore we decide to use here a more conservative selection, i.e. considering only galaxies lying within ±0.04 mag from the median values of r'–i' and i'–z' colors (see Fig. 13 with 272 galaxies with $r' < 20.8$). The galaxy distribution shows the N–S elongation of A1240 and the presence of A1237. Moreover, another cluster is shown at $\sim 25'$ South–East of A1240. This cluster was also detected by Gal et al. (2003) and Koester et al. (2007), who estimated a photometric $z \sim 0.18$–0.19.

4. X–ray analysis of A1240

The X–ray analysis of A1240 is performed on the archival data of the Chandra ACIS–I observation 800407 (exposure ID #4961). The pointing has an exposure time of 52 ks. Data reduc-

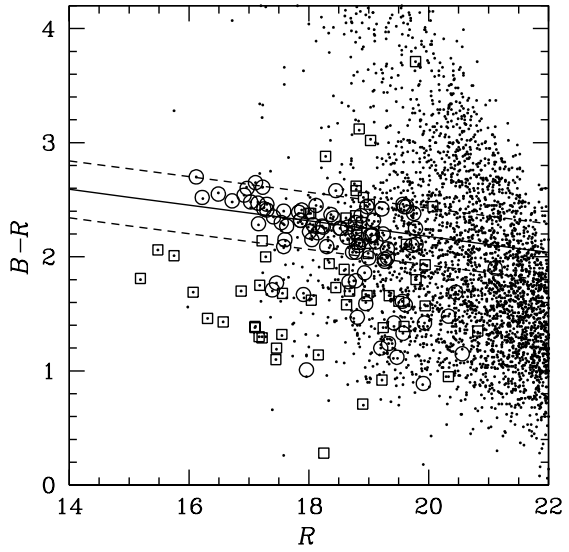

Fig. 11. *B–R* vs. *R* diagram for galaxies with available spectroscopy is shown by large circles and squares (members and non members, respectively). Small points indicate galaxies found in our INT photometric sample, i.e. objects with a class star ≤ 0.9. The solid line gives the best–fit color–magnitude relation as determined on spectroscopically confirmed member galaxies; the dashed lines are drawn at ±0.25 mag from the color–magnitude relation.

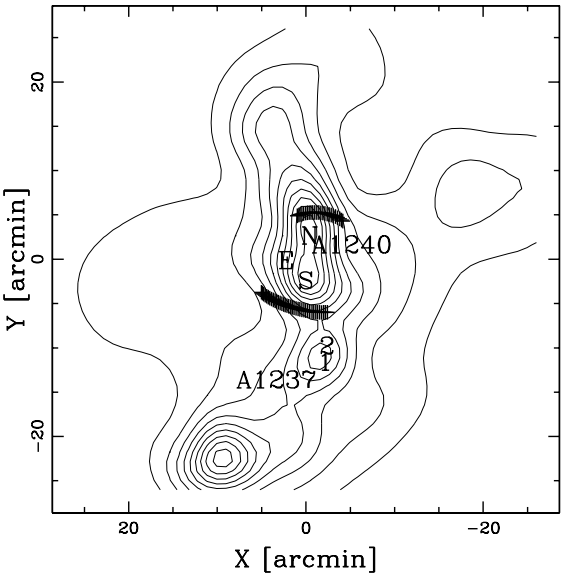

Fig. 13. Spatial distribution on the sky and relative isodensity contour map of likely cluster members (applying the color–color selection to the SDSS photometric catalog) with $r' \leq 20.8$, obtained with the DEDICA method. The positions of the brightest galaxies are indicated. The two relics are indicated in a schematic way.

tion is performed using the package CIAO[3] (Chandra Interactive Analysis of Observations) on chips I0, I1, I2 and I3 (field of view ~ 17′ × 17′). First, we remove events from the level 2 event list with a status not equal to zero and with grades one, five and seven. Then, we select all events with energy between 0.3 and 10 keV. In addition, we clean bad offsets and examine the data, filtering out bad columns and removing times when the count rate exceeds three standard deviations from the mean count rate per 3.3 s interval. We then clean the chips for flickering pixels, i.e., times where a pixel has events in two sequential 3.3 s intervals. The resulting exposure time for the reduced data is 51.3 ks.

[3] CIAO is freely available at http://asc.harvard.edu/ciao/

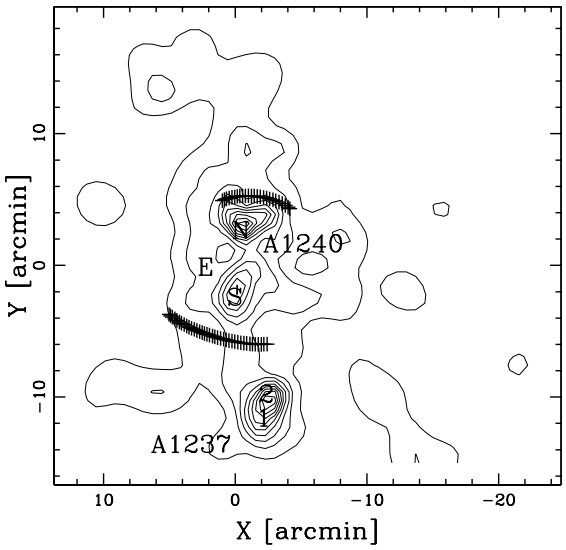

Fig. 12. Spatial distribution on the sky and relative isodensity contour map of likely cluster members (applying the color–magnitude selection to the INT photometric catalog) with $R \leq 20.5$, obtained with the DEDICA method. The positions of the brightest galaxies are indicated. The two relics are indicated in a schematic way.

A quick look of the reduced image is sufficient to have an hint of the morphology of the extended X–ray emission of A1240. However, the cluster was centered exactly in the "cross" of the gaps among the four chips. To obtain a more precise result, we have to correct the photon counts in the poorly exposed ACIS CCD gaps. First, we operate a binning of the reduced image. Then, we operate a soft smoothing and correct the photon counts with a division by an exposure map. The result is an image from which we extract the contour levels (soft photons in the energy range 0.5–2 keV) plotted in Fig. 1.

The complex X–ray morphology of A1240 is evident. In particular, the central X–ray emission is clearly elongated in the N–S direction, i.e. the same direction defined by the two galaxy clumps A1240N and A1240S. Contour levels in Fig. 1 also reveal a diffuse source ~6′ SE of the cluster center. A visual inspection of the INT *R*–band image shows that this structure does not match with any evident galaxy concentration. We suspect it could be a distant background galaxy group. Unfortunately, a more quantitative morphological analysis is not trivial. In fact, the gaps among the ACIS chips make quite critical the computation of the surface brightness distribution. Moreover, the disturbed morphology of the ICM does not justify the spherical symmetric assumption. This does not encourage the presentation of X-ray profiles.

As for the spectral properties of the cluster X–ray photons, we compute a global estimate of the ICM temperature. The tem-

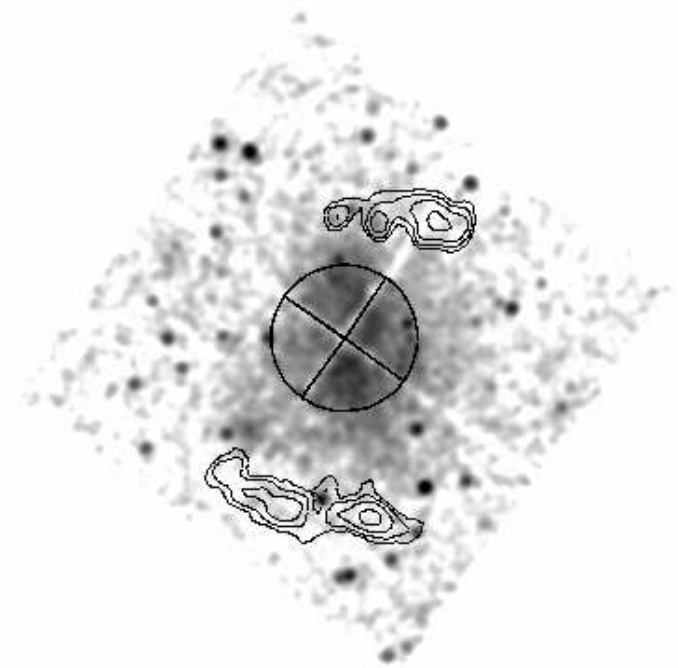

Fig. 14. 17′×17′ Chandra X–ray **smoothed** image (ID 4961) of A1240 in the energy band 0.5–2 keV (North at the top and East to the left). The central circle has a radius of ∼2.58′ (0.5 Mpc at the cluster redshift, see text). Black contours show the two radio relics.

perature is computed from the X–ray spectrum of the cluster within a circular aperture of ∼2.58′ radius (0.5 Mpc at the cluster redshift; see Fig. 14) around the center of the four ACIS chips. Fixing the absorbing galactic hydrogen column density at 1.99×10^{20} cm^{-2}, computed from the HI maps by Dickey & Lockman (1990), we fit a Raymond–Smith (1977) spectrum using the CIAO package Sherpa with a χ^2 statistics and assuming a metal abundance of 0.3 in solar units. We find a best fitting temperature of $T_{\rm X} = 6.0 \pm 0.5$ keV.

We then search for temperature gradients by dividing the 0.5 Mpc radius circle in four quadrants (chosen in order to avoid the gaps among the chips), as shown in Fig. 14. As expected for a merging cluster, there is some evidence that the ICM temperature is not homogeneous, with the Western quadrant ($T_{\rm X}$=$6.7^{+1.9}_{-1.2}$ keV) somewhat hotter than the Northern ($T_{\rm X}$=$5.1^{+1.0}_{-0.8}$ keV), the Eastern ($T_{\rm X}$=$5.2^{+1.9}_{-1.2}$ keV) and Southern ($T_{\rm X}$=$5.4^{+0.9}_{-0.8}$ keV) quadrants. More detailed temperature and metallicity maps would be highly desirable to better describe the properties of the ICM, but the photon statistics is not good enough to this aim. In particular, we do not provide any estimate of the ICM temperature in proximity of the two relics, where the X–ray surface brightness is too low to obtain any reliable measurement (see Fig. 14).

5. Cluster structure: discussion

Both optical and X–ray data indicate that A1240 is a strongly substructured cluster, elongated in the N–S direction, the same of the axis of symmetry of the relics. We also detect two clumps, separated by 1.2 h_{70}^{-1} Mpc, in the galaxy distribution. These observational features suggest that we are looking at a cluster just forming through the merging of two main subclumps. The difficulty in separating the two subclumps in the velocity space and the small LOS velocity difference of the two BCGs suggest that the axis of the merger lies in the plane of the sky. The evidence of a very disturbed ICM distribution, somewhat displaced from the galaxy distribution, suggests that the merger is seen after the phase of the core passage, as shown by the results of the numerical simulation (e.g., Roettiger et al. 1997, their Figs. 7–14).

As for the observational cluster structure, A1240 is similar to Abell 3667 (see Roettiger et al. 1999 and refs. therein) where the optical and X–ray structures are elongated in a direction roughly similar to that of the axis of symmetry of the two radio relics which are separated by $\sim 3-4\ h_{70}^{-1}$ Mpc. The two intervening galaxy subclumps are separated by $\sim 1\ h_{70}^{-1}$ Mpc with a small LOS velocity difference ~ 120 km s^{-1} between the dominant galaxies. Basic observational features of Abell 3667 were explained with the "outgoing merger shocks" model, where shocks provide sites for diffusive shock acceleration of relativistic electrons causing the presence of the radio sources (Roettiger et al. 1999).

For A1240 we have detected two galaxy subclumps in the N–S direction, the same direction of the elongation of the X–ray surface brightness and the axis of symmetry of the two radio relics. The values of relevant parameters for the two–clumps system, as deduced from the BCGN and BCGS, are: the relative LOS velocity in the rest–frame, $V_{\rm rf} = 390$ km s^{-1} , and the projected linear distance between the two clumps, $D = 1.2\ h_{70}^{-1}$ Mpc. The two roughly symmetric relics lie more externally, separated by a projected linear distance $\sim 2\ h_{70}^{-1}$ Mpc (Bonafede et al. 2009).

We now use the above parameters and the mass of the system computed in a range $M_{\rm A1240} = (0.9-1.9)\times10^{15}\ h_{70}^{-1}\ M_\odot$ to investigate the relative dynamics of A1240N and A1240S. In particular, we use different analytic approaches based on an energy integral formalism in the framework of locally flat spacetime and Newtonian gravity (e.g., Beers et al. 1982).

First, we compute the Newtonian criterion for gravitational binding stated in terms of the observables as $V_{\rm r}^2 D \leq 2GM_{\rm sys}\sin^2\alpha\cos\alpha$, where α is the projection angle between the plane of the sky and the line connecting the centers of the two clumps. The thin curve in Fig. 15 separates the bound and unbound regions according to the Newtonian criterion (above and below the curve, respectively). Considering the lower (upper) limit of $M_{\rm A1240}$, the N+S system is bound between 9° and 84° (6° and 89°); the corresponding probability, computed considering the solid angles (i.e., $\int_{\alpha1}^{\alpha2}\cos\alpha\, d\alpha$), is 84% (89%).

Then, we apply the analytical two–body model introduced by Beers et al. (1982) and Thompson (1982; see also Lubin et al. 1998 for a more recent application). This model assumes radial orbits for the clumps with no shear or net rotation of the system. According to the boundary conditions usually considered, the clumps are assumed to start their evolution at time $t_0 = 0$ with separation $d_0 = 0$, and now moving apart or coming together for the first time in their history.

In the case of A1240N+A1240S system, where the first core passage has likely already occurred, we assume that the time $t_0 = 0$ with separation $d_0 = 0$ is the time of their core crossing and that we are looking at the cluster a time t after. To obtain an estimate of t we use the Mach number of the shock $\mathcal{M} \sim 3$ as recovered by Bonafede et al. (2009) from the radio spectral index. The Mach number is defined as $\mathcal{M} = {\rm v_s}/c_{\rm s}$, where $\rm v_s$ is the velocity of the shock and $c_{\rm s}$ in the sound speed in the pre–shock gas (see e.g., Sarazin 2002 for a review). The value of $c_{\rm s}$, obtained from our estimate of $T_{\rm X}$, i.e. $c_{\rm s} \sim 995$ km s^{-1}, leads to a value of ${\rm v_s} \sim 3\times10^3$ km s^{-1}. Assuming the shock velocity as a constant, the shock covered a $\sim 1\ h_{70}^{-1}$ Mpc scale (i.e. the

distance of the relics from the cluster center) in a time of ~ 0.3 Gyrs. We assume this time as our estimate of t. Although the velocity of the shock is not constant, recent studies based on numerical simulations show how the variation of v_s is much smaller than the variation of the relative velocity of the subclumps identified with their dark matter components (see Fig. 4 of Springel & Farrar 2007; see Fig. 14 of Mastropietro & Burkert 2008), thus our rough estimate of t is acceptable at the first order of approximation.

The bimodal model solution gives the total system mass $M_{\rm sys}$ as a function of α (e.g., Gregory & Thompson 1984). Figure 15 compares the bimodal–model solutions with the observed mass of the system. The present solutions span the bound outgoing solutions (i.e. expanding), BO; the bound incoming solutions (i.e. collapsing), BI_a and BI_b; and the unbound outgoing solutions, UO. For the incoming case there are two solutions because of the ambiguity in the projection angle α. Both the BO and UO solutions are, in principle, consistent with the observed mass range. However, the BO solution is the more likely since the probability associated to the BO solution is much higher than that associated to the UO solution. In fact, we obtain that P(BO) and P(UO) are 92% and 8%, respectively, where these probabilities are computed considering the solid angles (see above) and assuming that the region of $M_{\rm sys}$ values is equally probable for individual solutions (see e.g. Barrena et al. 2007b). As for the projection angle we estimate a value of $\alpha \sim 10^\circ$. This small angle means that the real spatial distance between A1240 subclumps is similar to the projected one while the real, i.e. deprojected, velocity difference is $V_{\rm rf} \sim 2000$ km s^{-1}, a quite reasonable value during cluster mergers (see, e.g. Springel & Farrar 2007 and refs. therein). Notice that the relative velocity between galaxy clumps is smaller than the shock velocity, i.e. the regime is not stationary, but this is expected when comparing shock and collisionless components in numerical simulations (Springel & Farrar 2007; Mastropietro & Burkert 2008).

Since the merger of A1240 clumps occurred largely in the plane of the sky, this likely explains the similarity between the observational features of A1240 and Abell 3667. However, the case of A1240 is made more complex by the presence of A1237.

We investigate the relative dynamics of A1237 and A1240 with the same approach described above. The values of the relevant observable quantities for the two–clumps system are based on Table 2, i.e. LOS $V_{\rm rf} = 320$ km s^{-1} and $D = 2.7\ h_{70}^{-1}$ Mpc. For the mass of the system we use the mass range computed in Sect. 3.6, $M_{\rm A1237+A1240} = (15-25)\times10^{15}\ h_{70}^{-1}\ M_\odot$. The Newtonian criterion for gravitational binding leads to a system bound between 8° and 89° (7° and 89°); the corresponding probability, computed considering the solid angles (i.e., $\int_6^{89} \cos\alpha\, d\alpha$), is 87% (89%).

In the case of A1237 and A1240 we have no evidence of a previous merger since the gas distribution of A1240 (although very complex) does not show evidence of a peculiar displacement in direction of A1237. Therefore we assume that we are looking at A1237 and A1240 before their encounter. X–ray observations of A1237 would be useful to confirm this hypothesis. Under our assumption we can use the standard version of the analytical two–body model to study the A1237+A1240 system, where the clumps are assumed to start their evolution at time $t_0 = 0$ with separation $d_0 = 0$, and are moving apart or coming together for the first time in their history. We are looking at the system at the time of $t = 11.090$ Gyrs, i.e. the age of the Universe at the system redshift. The solutions consistent with the observed mass span these cases: the bound and present incoming solution (i.e. collapsing), BI_a and BI_b, and the bound–outgoing solution, BO (see Fig. 16). The associated probabilities are 61%, 31% and 8%, for BI_a, BI_b and BO respectively. The most probable solution is also the most interesting one since the BI_a solution gives the same value of $\alpha \sim 10^\circ$already found for the A1240N+S merger. In this case, the direction of the clump velocities are consistent, too: at the present time A1240N has already crossed A1240S, being now in front of A1240S and moving outgoing; A1237 is lying behind A1240 and is infalling onto it along almost the same N–S direction.

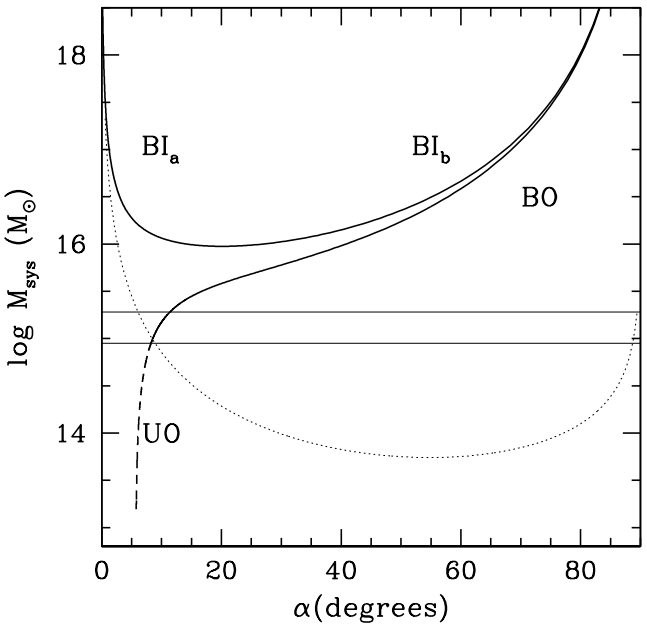

Fig. 15. System mass vs. projection angle for bound and unbound solutions (thick solid and thick dashed curves, respectively) of the two–body model applied to A1240N and A1240S subsystems. Labels BI_a and BI_b indicate the bound and incoming, i.e. collapsing solutions (thick solid curve). Label BO indicates the bound outgoing, i.e. expanding solutions (thick solid curve). Label UO indicates the unbound outgoing solutions (thick dashed curve). The horizontal lines give the range of observational values of the mass system. The thin dashed curve separates bound and unbound regions according to the Newtonian criterion (above and below the thin dashed curve, respectively).

6. Conclusions

Our results strongly support the conclusion of Bonafede et al. (2009), based on radio data, in favor of the "outgoing merger shocks" model for the double relics of A1240. In fact, we detect the intervening merging subclumps and recover an acceptable model for the internal cluster dynamics. Moreover, our results also suggest that we are looking at the cluster accretion along a large scale structure filament.

Our analysis shows how powerful is the study of the internal cluster dynamics through the analysis of kinematics of cluster galaxies. Other insights into A1240 might be recovered from a better knowledge of galaxy properties, e.g. spectral signatures of past activity which could be useful to determine the relevant time–scales (see e.g., Ferrari et al. 2003; Boschin et al. 2004)

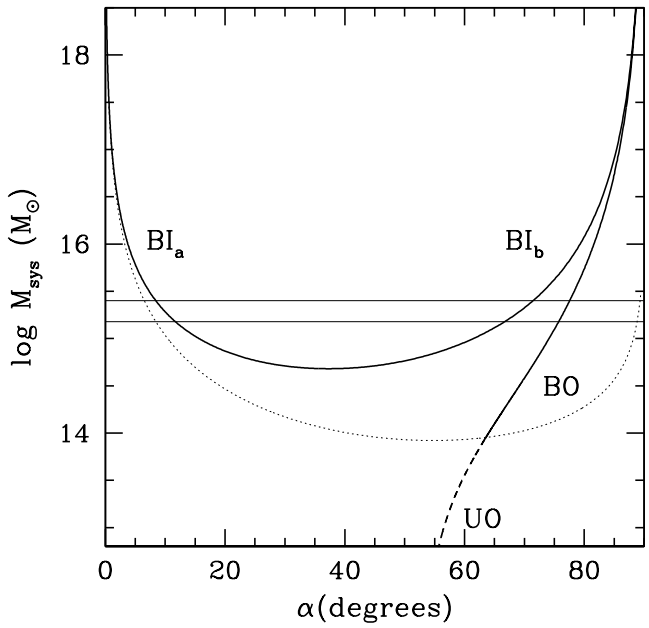

Fig. 16. System mass vs. projection angle for bound and unbound solutions (solid and dashed curves, respectively) of the two–body model applied to A1237 and A1240 systems.

and from deeper X–ray observations (see, e.g Vikhlinin et al. 2001 for the discover of a "cold front" in Abell 3667). Finally, we point out that A1240, with its displacement between collisional (gas) and collisionless components (galaxies), is an excellent candidate to study the properties of the dark matter, in particular its collisional cross section, as already performed in other merging clusters (Markevitch et al. 2004; Bradač et al. 2008).

Acknowledgements. We are in debt with Klaus Dolag for interesting discussions. We thank the anonymous referee for her/his useful suggestions. This publication is based on observations made on the island of La Palma with the Italian Telescopio Nazionale Galileo (TNG) and the Isaac Newton Telescope (INT). The TNG is operated by the Fundación Galileo Galilei – INAF (Istituto Nazionale di Astrofisica). The INT is operated by the Isaac Newton Group. Both telescopes are located in the Spanish Observatorio of the Roque de Los Muchachos of the Instituto de Astrofisica de Canarias.

This research has made use of the NASA/IPAC Extragalactic Database (NED), which is operated by the Jet Propulsion Laboratory, California Institute of Technology, under contract with the National Aeronautics and Space Administration.

This research has made use of the galaxy catalog of the Sloan Digital Sky Survey (SDSS). Funding for the SDSS has been provided by the Alfred P. Sloan Foundation, the Participating Institutions, the National Aeronautics and Space Administration, the National Science Foundation, the U.S. Department of Energy, the Japanese Monbukagakusho, and the Max Planck Society. The SDSS Web site is http://www.sdss.org/.

The SDSS is managed by the Astrophysical Research Consortium for the Participating Institutions. The Participating Institutions are the American Museum of Natural History, Astrophysical Institute Potsdam, University of Basel, University of Cambridge, Case Western Reserve University, University of Chicago, Drexel University, Fermilab, the Institute for Advanced Study, the Japan Participation Group, Johns Hopkins University, the Joint Institute for Nuclear Astrophysics, the Kavli Institute for Particle Astrophysics and Cosmology, the Korean Scientist Group, the Chinese Academy of Sciences (LAMOST), Los Alamos National Laboratory, the Max–Planck–Institute for Astronomy (MPIA), the Max–Planck–Institute for Astrophysics (MPA), New Mexico State University, Ohio State University, University of Pittsburgh, University of Portsmouth, Princeton University, the United States Naval Observatory, and the University of Washington.

References

Abell, G. O., Corwin, H. G. Jr., & Olowin, R. P. 1989, ApJS, 70, 1
Ashman, K. M., Bird, C. M., & Zepf, S. E. 1994, AJ, 108, 2348
Bagchi, J., Durret, F., Lima Neto, G. B., & Paul, S. 2006, Science, 314, 791
Bardelli, S., Zucca, E., Vettolani, G., et al. 1994, MNRAS, 267, 665
Barrena, R., Boschin, W., Girardi, M., & Spolaor, M. 2007a, A&A, 467, 37
Barrena, R., Boschin, W., Girardi, M., & Spolaor, M. 2007b, A&A, 469, 861
Beers, T. C., Flynn, K., & Gebhardt, K. 1990, AJ, 100, 32
Beers, T. C., Forman, W., Huchra, J. P., Jones, C., & Gebhardt, K. 1991, AJ, 102, 1581
Beers, T. C., & Geller, M. J. 1983, ApJ, 274, 491
Beers, T. C., Geller, M. J., & Huchra, J. P. 1982, ApJ, 257, 23
Bertin, E., & Arnouts, S. 1996, A&AS, 117, 393
Bird, C. M., & Beers, T. C. 1993, AJ, 105, 1596
Bonafede, A., Giovannini, G., Feretti, L., Govoni, F., & Murgia M. 2009, A&A, 494, 429
Boschin, W., Barrena, R., & Girardi, M. 2009, A&A, 495, 15
Boschin, W., Barrena, R., Girardi, M., & Spolaor, M. 2008, A&A, 487, 33
Boschin, W., Girardi, M., Barrena, R., et al. 2004, A&A, 416, 839
Boschin, W., Girardi, M., Spolaor, M., & Barrena, R. 2006, A&A, 449, 461
Bradač, M., Allen, S. W., Treu, T., et al. 2008, ApJ, 687, 959
Buote, D. A. 2002, in "Merging Processes in Galaxy Clusters", eds. L. Feretti, I. M. Gioia, & G. Giovannini (The Netherlands, Kluwer Ac. Pub.): Optical Analysis of Cluster Mergers
Burstein, D., & Heiles, C. 1982, AJ, 87, 1165
Carlberg, R. G., Yee, H. K. C., & Ellingson, E. 1997, ApJ, 478, 462
Cassano, R., & Brunetti, G. 2005, MNRAS, 357, 1313
Cousins, A. W. J., 1976, Mem. R. Astr. Soc, 81, 25
Danese, L., De Zotti, C., & di Tullio, G. 1980, A&A, 82, 322
David, L. P., Forman, W., & Jones, C. 1999, ApJ, 519, 533
Dickey, J. M., & Lockman, F. J. 1990, ARA&A, 28, 215
Dressler, A., & Shectman, S. A. 1988, AJ, 95, 985
Ebeling, H., Voges, W., Böhringer, H., et al. 1996, MNRAS, 281, 799
Ellingson, E., & Yee, H. K. C. 1994, ApJS, 92, 33
Ensslin, T. A., Biermann, P. L., Klein, U., & Kohle, S. 1998, A&A, 332, 395
Ensslin, T. A., & Gopal–Krishna 2001, A&A, 366, 26
Fadda, D., Girardi, M., Giuricin, G., Mardirossian, F., & Mezzetti, M. 1996, ApJ, 473, 670
Fasano, G., & Franceschini, A. 1987, MNRAS, 225, 155
Feretti, L. 2008, Mem. SAIt, 79, 176
Feretti, L. 2006, Proceedings of the XLIst Rencontres de Moriond, XXVIth Astrophysics Moriond Meeting: "From dark halos to light", L.Tresse, S. Maurogordato and J. Tran Thanh Van, Eds, e-print astro-ph/0612185
Feretti, L. 1999, MPE Report No. 271
Feretti, L. 2002a, The Universe at Low Radio Frequencies, Proceedings of IAU Symposium 199, held 30 Nov – 4 Dec 1999, Pune, India. Edited by A. Pramesh Rao, G. Swarup, and Gopal–Krishna, 2002., p.133
Feretti, L. 2005a, X–Ray and Radio Connections (eds. L. O. Sjouwerman and K. K. Dyer). Published electronically by NRAO, http://www.aoc.nrao.edu/events/xraydio. Held 3–6 February 2004 in Santa Fe, New Mexico, USA
Feretti, L., Gioia I. M., and Giovannini G. eds., 2002b, Astrophysics and Space Science Library, vol. 272 "Merging Processes in Galaxy Clusters", Kluwer Academic Publisher, The Netherlands
Feretti, L., Schuecker, P., Böehringer, H., Govoni, F., & Giovannini, G. 2005b, A&A, 444, 157
Ferrari, C., Govoni, F., Schindler, S., Bykov, A. M., & Rephaeli, Y. 2008, Space Sci. Rev., 134, 93
Ferrari, C., Maurogordato, S., Cappi, A., & Benoist C. 2003, A&A, 399, 813
Flores, R. A., Quintana, H., & Way, M. J. 2000, ApJ, 532, 206
Gal, R. R., de Carvalho, R. R., Lopes, P. A. A., et al. 2003, AJ, 125, 2064
Giovannini, G., & Feretti, L. 2002, in "Merging Processes in Galaxy Clusters", eds. L. Feretti, I. M. Gioia, & G. Giovannini (The Netherlands, Kluwer Ac. Pub.): Diffuse Radio Sources and Cluster Mergers
Giovannini, G., Tordi, M., & Feretti, L. 1999, New Astronomy, 4, 141
Girardi, M., Barrena, R., and Boschin, W. 2007, Contribution to "Tracing Cosmic Evolution with Clusters of Galaxies: Six Years Later" conference – http://www.si.inaf.it/sesto2007/contributions/Girardi.pdf
Girardi, M., & Biviano, A. 2002, in "Merging Processes in Galaxy Clusters", eds. L. Feretti, I. M. Gioia, & G. Giovannini (The Netherlands, Kluwer Ac. Pub.): Optical Analysis of Cluster Mergers
Girardi, M., Biviano, A., Giuricin, G., Mardirossian, F., & Mezzetti, M. 1995, ApJ, 438, 527
Girardi, M., Escalera, E., Fadda, D., et al. 1997, ApJ, 482, 11
Girardi, M., Fadda, D., Giuricin, G. et al. 1996, ApJ, 457, 61
Girardi, M., Giuricin, G., Mardirossian, F., Mezzetti, M., & Boschin, W. 1998, ApJ, 505, 74

Girardi, M., & Mezzetti, M. 2001, ApJ, 548, 79
Goto, T., Sekiguchi, M., Nichol, R. C., et al. 2002, AJ, 123, 1807
Gregory, S. A., & Thompson, L. A. 1984, ApJ, 286, 422
Gullixson, C. A. 1992, in "Astronomical CCD Observing and Reduction techniques" (ed. S. B. Howell), ASP Conf. Ser., 23, 130
Hoeft, M., Brüggen, M., & Yepes, G. 2004, MNRAS, 347, 389
Johnson, H. L., & Morgan, W. W. 1953, ApJ, 117, 313
Kempner, J. C., Blanton, E. L., Clarke, T. E. et al. 2003, Proceedings of "The Riddle of Cooling Flows in Galaxies and Clusters of Galaxies", eds. T. H. Reiprich, J. C. Kempner, & N. Soker, e-print astro-ph/0310263
Kempner, J. C., & Sarazin, C. L. 2001, ApJ, 548, 639
Kennicutt, R. C. 1992, ApJS, 79, 225
Koester, B. P., McKay, T. A., Annis, J., et al. 2007, ApJ, 660, 239
Limber, D. N., & Mathews, W. G. 1960, ApJ, 132, 286
López–Cruz, O., Barkhouse, W. A., & Yee, H. K. C. 2004, ApJ, 614, 679
Lubin, L. M., Postman, M., & Oke, J. B. 1998, AJ, 116, 643
Malumuth, E. M., Kriss, G. A., Dixon, W. Van Dyke, Ferguson, H. C., & Ritchie, C. 1992, AJ, 104, 495
Markevitch, M., Gonzalez, A. H., Clowe, D., et al. 2004, ApJ, 606, 819
Mastropietro, C., & Burkert, A. 2008, MNRAS, 389, 967
Mazure, A., Proust, D., Mathez, G., & Mellier, Y. 1988, A&AS, 76, 339
Pisani, A. 1993, MNRAS, 265, 706
Pisani, A. 1996, MNRAS, 278, 697
Poggianti, B. M. 1997, A&AS, 122, 399
Press, W. H., Teukolsky, S. A., Vetterling, W. T., & Flannery, B. P. 1992, in Numerical Recipes (Second Edition), (Cambridge University Press)
Quintana, H., Carrasco, E. R., & Reisenegger, A. 2000, AJ, 120, 511
Quintana, H., Ramírez, A., & Way, M. J. 1996, AJ, 112, 360
Raymond, J. C., & Smith, B. W. 1977, ApJS, 35, 419
Roettiger, K., Burns, J. O., & Stone, J. M. 1999, ApJ, 518, 603
Roettiger, K., Loken, C., & Burns, J. O. 1997, ApJS, 109, 307
Röttgering, H. J. A., Wieringa, M. H., Hunstead, R. W., & Ekers, R. D. 1997, MNRAS, 290, 577
Sarazin, C. L. 2002, in "Merging Processes in Galaxy Clusters", eds. L. Feretti, I. M. Gioia, & G. Giovannini (The Netherlands, Kluwer Ac. Pub.): The Physics of Cluster Mergers
Springel, V., & Farrar, G. R. 2007, MNRAS, 380, 911
The, L. S., & White, S. D. M. 1986, AJ, 92, 1248
Thompson, L. A. 1982, in IAU Symposium 104, Early Evolution of the Universe and the Present Structure, eds. G.O. Abell and G. Chincarini (Dordrecht: Reidel)
Tonry, J., & Davis, M. 1979, ApJ, 84, 1511
Venturi, T., Giacintucci, S., Brunetti, G., et al. 2007, A&A, 4363, 937
Vikhlinin, A., Markevitch, M., & Murray, S. S. 2001, ApJ, 551, 160
Visvanathan, N., & Sandage, A. 1977, ApJ, 216, 214
Wainer, H., & Schacht, S. 1978, Psychometrika, 43, 203

List of Objects

'Abell 1240' on page 2
'Abell 1237' on page 2